



UNIVERSIDAD DE INVESTIGACIÓN DE TECNOLOGÍA EXPERIMENTAL YACHAY

Escuela de Ciencias Biológicas e Ingeniería

TÍTULO: PREVENTING BACTERIAL FOULING USING BIO- FRIENDLY AND CONDUCTIVE THIN-FILMS BASED ON GRAPHENE

Trabajo de integración curricular presentado como requisito para la
obtención del título de Ingeniera Biomédica

Autor:

Chicaiza Zambrano Alanis

Tutor:

Ph.D – Alexis Frank

Co-tutor:

Ph.D – Zamora- Ledezma Camilo

Urcuquí, marzo 2020

SECRETARÍA GENERAL
(Vicerrectorado Académico/Cancillería)
ESCUELA DE CIENCIAS BIOLÓGICAS E INGENIERÍA
CARRERA DE BIOMEDICINA
ACTA DE DEFENSA No. UITEY-BIO-2020-00015-AD

A los 15 días del mes de mayo de 2020, a las 16:30 horas, de manera virtual mediante videoconferencia, y ante el Tribunal Calificador, integrado por los docentes:

Presidente Tribunal de Defensa	<u>Dra. SALUM , GRACIELA MARISA , Ph.D.</u>
Miembro No Tutor	<u>Dr. SANTIAGO VISPO, NELSON FRANCISCO , Ph.D.</u>
Tutor	<u>Dr. ALEXIS FRANK , Ph.D.</u>

El(la) señor(ita) estudiante **CHICAIZA ZAMBRANO, ALANIS CECILIA**, con cédula de identidad No. 1717593386, de la ESCUELA DE CIENCIAS BIOLÓGICAS E INGENIERÍA, de la Carrera de BIOMEDICINA, aprobada por el Consejo de Educación Superior (CES), mediante Resolución RPC-SO-43-No.496-2014, realiza a través de videoconferencia, la sustentación de su trabajo de titulación denominado: **Preventing bacterial fouling using bio-friendly and conductive Thin-films based on Graphene**, previa a la obtención del título de INGENIERO/A BIOMÉDICO/A.

El citado trabajo de titulación, fue debidamente aprobado por el(los) docente(s):

Tutor Dr. ALEXIS FRANK , Ph.D.

Y recibió las observaciones de los otros miembros del Tribunal Calificador, las mismas que han sido incorporadas por el(la) estudiante.

Previamente cumplidos los requisitos legales y reglamentarios, el trabajo de titulación fue sustentado por el(la) estudiante y examinado por los miembros del Tribunal Calificador. Escuchada la sustentación del trabajo de titulación a través de videoconferencia, que integró la exposición de el(la) estudiante sobre el contenido de la misma y las preguntas formuladas por los miembros del Tribunal, se califica la sustentación del trabajo de titulación con las siguientes calificaciones:

Tipo	Docente	Calificación
Tutor	Dr. ALEXIS FRANK , Ph.D.	10.0
Presidente Tribunal De Defensa	Dra. SALUM , GRACIELA MARISA , Ph.D.	10.0
Miembro Tribunal De Defensa	Dr. SANTIAGO VISPO, NELSON FRANCISCO , Ph.D.	10.0

Lo que da un promedio de: 10 (Diez punto Cero), sobre 10 (diez), equivalente a: **APROBADO**

Para constancia de lo actuado, firman los miembros del Tribunal Calificador, el(la) estudiante y el(la) secretario ad-hoc.

Certifico que *en cumplimiento del Decreto Ejecutivo 1017 de 16 de marzo de 2020, la defensa de trabajo de titulación (o examen de grado modalidad teórico práctica) se realizó vía virtual, por lo que las firmas de los miembros del Tribunal de Defensa de Grado, constan en forma digital.*

CHICAIZA ZAMBRANO, ALANIS CECILIA
Estudiante

Dra. SALUM , GRACIELA MARISA , Ph.D.
Presidente Tribunal de Defensa

Firmado digitalmente por
GRACIELA MARISA SALUM
 Fecha: 2020.07.13
 19:10:38 -05'00'

Dr. ALEXIS FRANK , Ph.D.
Tutor



Firmado digitalmente por
FRANK ALEXIS



Dr. SANTIAGO VISPO, NELSON FRANCISCO , Ph.D.
Miembro No Tutor



ALARCON FELIX, KARLA ESTEFANIA
Secretario Ad-hoc

AUTORÍA

Yo, **ALANIS CECILIA CHICAIZA ZAMBRANO**, con cédula de identidad 1717593386, declaro que las ideas, juicios, valoraciones, interpretaciones, consultas bibliográficas, definiciones y conceptualizaciones expuestas en el presente trabajo; así como, los procedimientos y herramientas utilizadas en la investigación, son de absoluta responsabilidad de el/la autor(a) del trabajo de integración curricular. Así mismo, me acojo a los reglamentos internos de la Universidad de Investigación de Tecnología Experimental Yachay.

Urququí, marzo 2020



Alanis Cecilia Chicaiza Zambrano
CI: 1717593386

AUTORIZACIÓN DE PUBLICACIÓN

Yo, **ALANIS CECILIA CHICAIZA ZAMBRANO**, con cédula de identidad 1717593386, cedo a la Universidad de Tecnología Experimental Yachay, los derechos de publicación de la presente obra, sin que deba haber un reconocimiento económico por este concepto. Declaro además que el texto del presente trabajo de titulación no podrá ser cedido a ninguna empresa editorial para su publicación u otros fines, sin contar previamente con la autorización escrita de la Universidad.

Asimismo, autorizo a la Universidad que realice la digitalización y publicación de este trabajo de integración curricular en el repositorio virtual, de conformidad a lo dispuesto en el Art. 144 de la Ley Orgánica de Educación Superior

Urcuquí, marzo 2020



Alanis Cecilia Chicaiza Zambrano
CI: 1717593386

Dedication

This thesis is dedicated:

To my parents, Nelly and Marco, who have always supported me, thank you for not letting me give up and inspiring me to be a better person every day with your patience, love, and teachings.

To my twin brothers Marcos and Fernanda, whom I consider my children, for being my accomplices and giving me a reason to smile every day.

My lovely grandmother, Lilia, for being my second mother and for guiding me with her life advice, without her none of this, would have been possible.

Finally, I want to thank the only person who allowed me to be myself and firmly believed in me, thanks to Carlos for being my person.

Alanis Cecilia Chicaiza Zambrano

Acknowledgment

I would like to thank the collaboration of several people who participated in the development of this research work. First, I would like to thank the professors of Yachay Tech University for giving us their knowledge and never giving up on their students.

Especially my tutor, Ph.D. Frank Alexis, and my co-author Ph.D. Camilo Zamora-Ledezma for helping me in my degree research, guide me and correct my mistakes. I want them to know that I want to dedicate my academic life to this topic.

Also, I would like to express my gratitude to the institutions that opened their doors and collaborated with my research; to the University of the Armed Forces (ESPE) and the National Polytechnic School. Thanks for all the information and help provided.

To Yachay University for earning the number 1 position in research and being my alma mater.

Alanis Cecilia Chicaiza Zambrano

Abstract

The development of novel and non-invasive treatments to prevent microorganism's adhesion and biofilm formation in medical prosthesis has become a challenge. This problem is mainly because, in the last decade, bacteria have been modifying their metabolic states, making them resistant even to the action of antibiotics.

For this reason, surface engineering is working with graphene coatings for the sterilization and improvement of biomedical implants surface since it has excellent physicochemical properties. In this work, we propose an innovative treatment based on the application of variable frequencies through thin-films based on graphene and poly (lactic-co-glycolic acid) (PLGA) to avoid the bacterial adhesion and biofilm formation. Furthermore, we tested their potential applications to prevent the growth of Escherichia Coli bacteria of the TG1 strain (*E. coli TG1*) as a function of the applied frequencies in the range $5 \text{ MHz} < f < 15 \text{ MHz}$. At this frequency, we did observe a "radio frequency bioelectric effect" that affected the polar parts of the microorganisms. The evaluation of the bactericidal effectiveness of this method was carried out following the typical process of dilution, measuring both the Optical Density at 600 nm and the Colony Forming Units (CFU). Our findings show improved bacteria annihilation when exposed to radiofrequency between 10MHz and 15MHz. We attribute this behavior to the fact that some cell walls were damaged when bacteria were exposed to a specific frequency. These results are promising to apply radiofrequency as an alternative and non-invasive method to prevent the formation of prosthetic biofilms.

Key-words: biofilm, graphene, thin-films, antibacterial, radiofrequency

Resumen

El desarrollo de tratamientos novedosos y no invasivos para prevenir la adhesión de microorganismos y la formación de biopelículas en prótesis médicas se ha convertido en un desafío. Este problema se debe principalmente a que, en la última década, las bacterias han estado modificando sus estados metabólicos, haciéndolas resistentes incluso a la acción de los antibióticos.

Por esta razón, la ingeniería de superficies está trabajando con recubrimientos de grafeno para la esterilización y mejora de la superficie de los implantes biomédicos, ya que tiene excelentes propiedades fisicoquímicas. En este trabajo, proponemos un tratamiento innovador basado en la aplicación de frecuencias variables a través de películas delgadas basadas en grafeno y poli (ácido láctico-co-glicólico) (PLGA) para evitar la adhesión bacteriana y la formación de biopelículas. Además, probamos sus aplicaciones potenciales para prevenir el crecimiento de la bacteria *Escherichia Coli* de la cepa TG1 (*E. coli* TG1) en función de las frecuencias aplicadas en el rango de 5 MHz <math><f < 15\text{ MHz}</math>. A esta frecuencia, observamos un "efecto bioeléctrico de radiofrecuencia" que afectó las partes polares de los microorganismos. La evaluación de la eficacia bactericida de este método se llevó a cabo siguiendo el proceso típico de dilución, midiendo tanto la densidad óptica a 600 nm como las unidades formadoras de colonias (UFC). Nuestros hallazgos muestran una mejor aniquilación de bacterias cuando se exponen a radiofrecuencia entre 10MHz y 15MHz. Atribuimos este comportamiento al hecho de que algunas paredes celulares fueron dañadas cuando las bacterias fueron expuestas a una frecuencia específica. Estos resultados son prometedores para aplicar la radiofrecuencia como un método alternativo y no invasivo para prevenir la formación de biopelículas protésicas.

Palabras clave: biopelícula, grafeno, películas delgadas, antibacteriano, radiofrecuencia

Index

1. Introduction: Theoretical framework	1
1.1 Prosthetic Joint Infection	1
1.2 Epidemiology	1
1.3 Classification.....	3
1.4 Pathology and Microbiology.....	3
1.5 How to treat Prosthetic Biofilm	6
1.6 Graphene in RF Applications.....	7
1.7 Graphene coatings in biomedical implants	7
1.8 Introduction to Graphene	8
1.9 Graphene Properties.....	9
1.9.1 Physical and mechanical properties	10
1.9.2 Biological Properties.....	11
2. Problem Statement	11
2.1 Infection associated with prosthetic joints in Ecuador	12
3. Hypothesis, General and Specific Objectives	15
3.1 Hypothesis.....	15
3.2 General Objective	15
3.3 Specific Objectives	15
4. Methodology	16
4.1 Materials	16
4.2 Culture Medium Preparation.....	17
4.3 Bacteria Preparation.....	18
4.4 Graphene Thin-films fabrication.....	19
4.5 Graphene Thin-films Characterization	21
4.6 Conductivity Experimental Setup	21
4.7 Effect of Electric field on Escherichia coli TG1 Growth	22
4.8 Structural and morphological Characterization of Escherichia Coli TG1/Graphene/PLGA thin-films	23
4.9 Statistical Test.....	23
5. Results	24
5.1. Graphene/PLGA Thin-films Characterization	24
5.2. Antibacterial Test.....	33
5.3. Statistical Analysis.....	40
6. Discussion	43
7. Conclusions, recommendations, and future work.	45
7.1 Conclusions.....	46
7.2 Recommendations and future work	47
Annex A	51
Annex B	52
Annex C	54

List of Tables

Table 1. % of Joint Prosthetic Infection Incidence	2
Table 2. Unique properties of Graphene as materials.....	10
Table 3. Absorbance values of the culture medium at 600 nm 1-hour after the RF treatment.....	33
Table 4. Absorbance values of the culture medium at 600 nm 12-hours after the RF treatment .	35
Table 5. Colony count of E. Coli TG1 per plate.....	36
Table 6. Bacteria survival Analysis	37
Table 7. Colony Forming Units (CFUs) Values	38
Table 8. Number of cell colonies and absorbance values	39
Table 9. Summary of statistical information concerning each group observations	40
Table 10. Summary of the ANOVA test.....	41
Table 11. Summary of pairwise t-test comparison of observation	42
Table 12. Levene's Test for Homogeneity of Variance	42
Table 13. Shapiro-Wilk normality test.....	43
Table 14. Optical Density values for each dilution at different frequency treatments	53
Table 15. Raw Data used for the statistical analysis in R.....	55

List of Graphs

Graph 1. Incidence of Osteoarthritis in Ecuador	14
Graph 2. XPS spectra for graphene powder (Gr), PLGA powder and, a PLGA/Gr thin film.....	29
Graph 3. Raman spectra for (i) a graphene powder (Gr), (ii) a PLGA powder, and (iii) a PLGA/Gr thin film.....	32
Graph 4. Absorbance measurement of the culture medium at 600 nm 1-hour after the RF treatment	34
Graph 5. Absorbance measurement of the culture medium at 600 nm 12-hours after the RF treatment	35
Graph 6. The survival rate of bacteria after the RF treatment at different frequency values	37
Graph 7. Measurement of the CFUs concerning the different radiofrequency treatments	38
Graph 8. Relationship between the number of cell colonies and absorbance values	39
Graph 9. Average values for each treatment concerning their absorbance values	41
Graph 10. Representation of the OD values at 600 nm for each dilution at different frequency treatments.....	54

List of Figures

Figure 1. Bacteria and biofilm distribution in a periprosthetic joint infection.	5
Figure 2. The 2D graphene is the building block of carbon materials of all dimensionalities: 0D,1D, and 3D	8
Figure 3. SEM morphologies of Thin-films based on Graphene.....	25
Figure 4. TEM cross-sectional structure of Thin-films based on Graphene.....	27
Figure 5. Graphene dispersions.....	28
Figure 6. SEM characterization of E. Coli TG1 bacteria.....	44
Figure 7. Magnification of dead E. Coli TG1 bacteria	44
Figure 8. Variable frequency experimental set up used to stimulate bacteria.	51
Figure 9. Method of dilution method and plate colony count.....	53

List of Schemes

Scheme 1. Flow-chart of the objectives of this investigation	16
Scheme 2. Preparation of solid and liquid culture medium and E. Coli bacteria incubation	18
Scheme 3. Graphene Thin-films Preparation.....	20
Scheme 4. Schematic configuration and main elements of the variable frequency experimental set up used to stimulate bacteria.	22

1. Introduction: Theoretical framework

1.1 Prosthetic Joint Infection

Prosthetic joint infection (PJI) is an increasing problem that mostly affects the elderly who have received a joint replacement. Especially in orthopedics, where 1.5%-2.5% of all the hip and knee arthroplasties will become infected. In the case of chronic and persistent deep tissue infection, the patient may require revision surgery or even amputation. The treatment costs the patient to the sender of US \$ 50,000, and the mortality can be as high as 2.5% (Webster, 2009).

PJI is defined as the infection that affects the tissue adjacent to the prosthesis (Tande & Patel, 2014). Numerous infections in implantable devices have been reported due to biofilm formation resistant even to the action of antibiotics and the host's immune response (Cacaci et al., 2019).

The contact of a microorganism with the prosthetic surface causes the PJI. The microorganisms reach the surface if the prosthesis in a direct way or by the hematogenic way. The most frequent is the direct way contamination in the surgery moment due to the presence of microorganisms in the patient skin, in the operating room, or the hospital staff (Oliete et al., 2015).

1.2 Epidemiology

The demand for joint replacement has increased in the last decade. This procedure improves the lives of millions of people around the world every year, relieves pain, restores the patient's function and independence.

In the United States, about one million total knees (TKA) and hip (THA) arthroplasties are performed annually, and it is estimated to quadruple by 2030. The condition rate ranges from 0.5 to 2% for knee replacements and 0.5 to 1% for hip replacements (Ayoade & Todd, 2019).

European countries, which participate in the ECDC's Surgical Site Infection (SSI) Surveillance network (HAI-Net), prosthetic infection rates average 0.8% in knee replacements and 1.5% for hip replacement (Sebastian et al., 2018). The majority of infections occurred within the first 30 days after surgery. Of the infections detected during the first year, 42% were classified as superficial, 43% as deep, and 15% as organic/spatial infections (Lamagni, 2014).

The information reported in hospitals in Latin America is scarce. However, different cases of prosthetic infection were reported; in Chile with an average of 2.5% for hip replacements and in Mexico with a percentage of 3.7% to 4.3% for knee replacements (Franco-Cendejas et al., 2017).

Table 1 contains the percentages of joint prosthetic infections according to different areas of the world (EE. UU, Europe, and South America). Remarkably, South American countries need more attention and data to specify the severity of infections in patients receiving joint prostheses.

While the average number of prosthetic infections increases, giving a sense of risk for patients undergoing arthroplasty, the real burden is evident through the evaluation of the economic and social impact on patients and hospital facilities. The overall cost to treat PJI was US \$566 million in 2009 alone, a number that is projected to reach USD 1.62 billion in 2020. Just taking into account the hospital cost and neglecting many other direct and indirect expenses (Tande & Patel, 2014).

Table 1. % of Joint Prosthetic Infection Incidence

Region	% Incidence of Joint Prosthetic Infection	
	Knee replacement (TKA)	Hip replacement (THA)
North America (Ayoade & Todd, 2019).	0.5%-2%	0.5%-1%
Europe	0.8%	1.5%

(Sebastian et al., 2018).		
South America (Tande & Patel, 2014) .	3.7%-4.3%	2.5%

1.3 Classification

There are many types of prosthetic infection; the most basic classification of PJI depends on the post-operative time of disease:

- *Early infection* occurs within the first three months,
- *Delayed infection* occurs between 3 and 24 months, and
- *Late infection* originates after 24 months.

McPherson and his colleagues established another type of classification. This classification is based on categorizing the type of infection (early postoperative infection Type I, hematogenous infection Type II, and late chronic infection Type III); the kind of host (A uncompromised, B compromised, and C significant compromised); and local limb conditions (1 uncompromised, 2 compromised, and 3 significant compromised) (Tande & Patel, 2014).

1.4 Pathology and Microbiology

There are two routes of entry of pathogenic bacteria; the direct route and the hematogenous route. The straightforward way is characterized by being a type of trans-operative infection (through the surgical incision). At the same time, the hematogenous way is the infection that occurs in the post-operative time of an area distant from the infection (Oliete et al., 2015).

High virulence bacteria cause early infection, and low virulence bacteria cause late infections. Microorganisms that cause PJI include coagulase-negative staphylococci (30-43%), *Staphylococcus aureus* (12-23%), streptococci (9-10%), enterococci (3-7%), gram-negative organisms (3- 6%) or anaerobes (2-4%) (McConoughey et al., 2014).

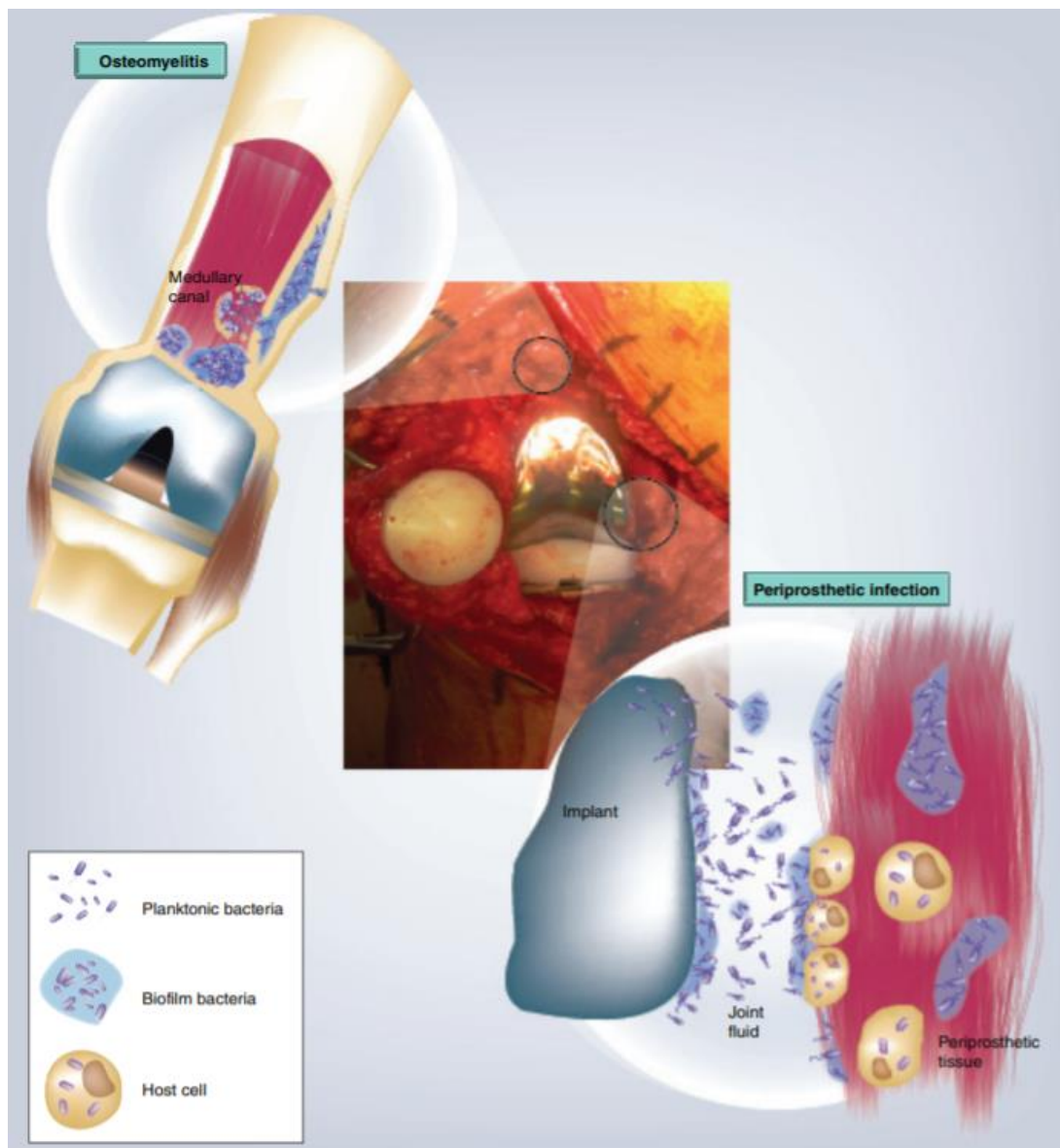
Once a small number of microorganisms reach the surface of the prosthesis, they multiply and form a layer known as a biofilm.

Biofilm

A biofilm is a community of bacteria within a polymer matrix that are bound to each other to a surface or are bound with host-derived proteins (Gilbertie et al., 2019)

The dynamics of biofilm formation helps microorganisms, in their starvation state, so that they can adhere to biotic and abiotic surfaces and survive for long periods on the surface, without the need for a nutrient-rich medium (Cacaci et al., 2019).

Figure 1. Bacteria and biofilm distribution in a periprosthetic joint infection



Source: (McConoughey et al., 2014)

The formed biofilm is composed of cells embedded in a matrix of extracellular polymeric substances (EPS) formed by proteins, polysaccharides, and nucleic acids (Caubet et al., 2004). The EPS matrix causes the biofilm to become relatively impermeable and gives resistance to the bacterial population by improving their metabolic states (Flemming & Wingender, 2010; Taylor

& Webster, n.d.).

In Figure 1, the process of the formation of prosthetic biofilm in a knee replacement can be observed. The process begins with the creation of an extracellular matrix (EPS) produced by a single Platonic bacterium. This matrix increases the adhesion of other neighboring microbes that become a highly organized collection of bacteria. In the maturation phase, bacteria become tolerant of antibiotics, and the extracellular matrix of polysaccharides, DNA, and proteins adhere to the surface of the prosthesis and adjacent tissue (McConoughey et al., 2014).

1.5 How to treat Prosthetic Biofilm

The treatments for bacterial infections and biofilm formation are based on different methods. For example, they are improving the efficiency of conventional antibiotics and on the application of new alternative treatments such as the use of immunotherapy, nanoparticles, lithic bacteriophages, photodynamic therapy, antimicrobial peptides, current, among others (Kiedrowski & Horswill, 2011; Liu et al., 2019).

1.1.1 Radiofrequency to treat prosthetic biofilm

The bioelectric effect implies an attack line to combat biofilm formation. This phenomenon has been tested in several types of biofilms (*Pseudomonas aeruginosa*, *Staphylococcus*, *Candida albicans*, *Klebsiella pneumoniae*, among others). The modified explanations of the bioelectric effect are based on the application of direct current (DC) and direct (DC) with electrodes, the modification of the pH, or the production of biocides by electrolysis (Caubet et al., 2004).

According to the literature, by replacing the DC with a radiofrequency current (RFC) with the same intensity, there is no ion transport between the electrodes, and no new ions or electrolysis are

created. However, a radio frequency bioelectric effect is created that affects the polar parts of the molecules forming the biofilm matrix (Caubet et al., 2004).

The application of variable frequency to create a low magnitude electric field promises to be a novel and non-invasive strategy to eliminate biofilms that could be integrated into clinical care (Taha et al., 2018).

1.6 Graphene in RF Applications

Applications in which radio frequency (RF) transmission is needed, benefits from the high mobility of carriers of materials such as graphene. The electrical conductivity of graphene is not affected by impurities or chemical impurities, causing charge carriers in the graphene to have long, half-free routes before encountering a dispersion event. On the other hand, common metals have impurities that disperse electrons, which dissipates energy. Therefore, the unique electronic transport characteristics of graphene make it very promising in RF applications (Aliofkhazraei et al., 2016).

1.7 Graphene coatings in biomedical implants

The utilization of mechanical properties of graphene has great potential when they act as biologically active functional surfaces. Due to its rigidity and strength, graphene is the ideal material for the manufacture of scaffolds and coatings in biomedical bone implants (Lee, Kim, & Shim, 2013).

The materials currently used in biomedical implants are based on alloys such as nitinol (NiTi) and stainless steel. These materials have excellent mechanical properties. However, they have insufficient biocompatibility and hemocompatibility and may even have cytotoxicity. (Bansiddhi et al., 2008; Podila et al., 2013).

The rejection of the material is mainly due to the lack of adhesion, proliferation, and cell growth. Implant contact with living cells activate the immune response and could cause an infection. Then, a coating that is biocompatible and improves the properties of currently used metal materials is needed. Graphene promises to be an excellent material for the surface of biomedical implants. Moreover, graphene has been shown to promote cell growth and proliferation, inhibits the platelet activation by implants, and is hemocompatible (Podila, Moore, Alexis, & Rao, 2013).

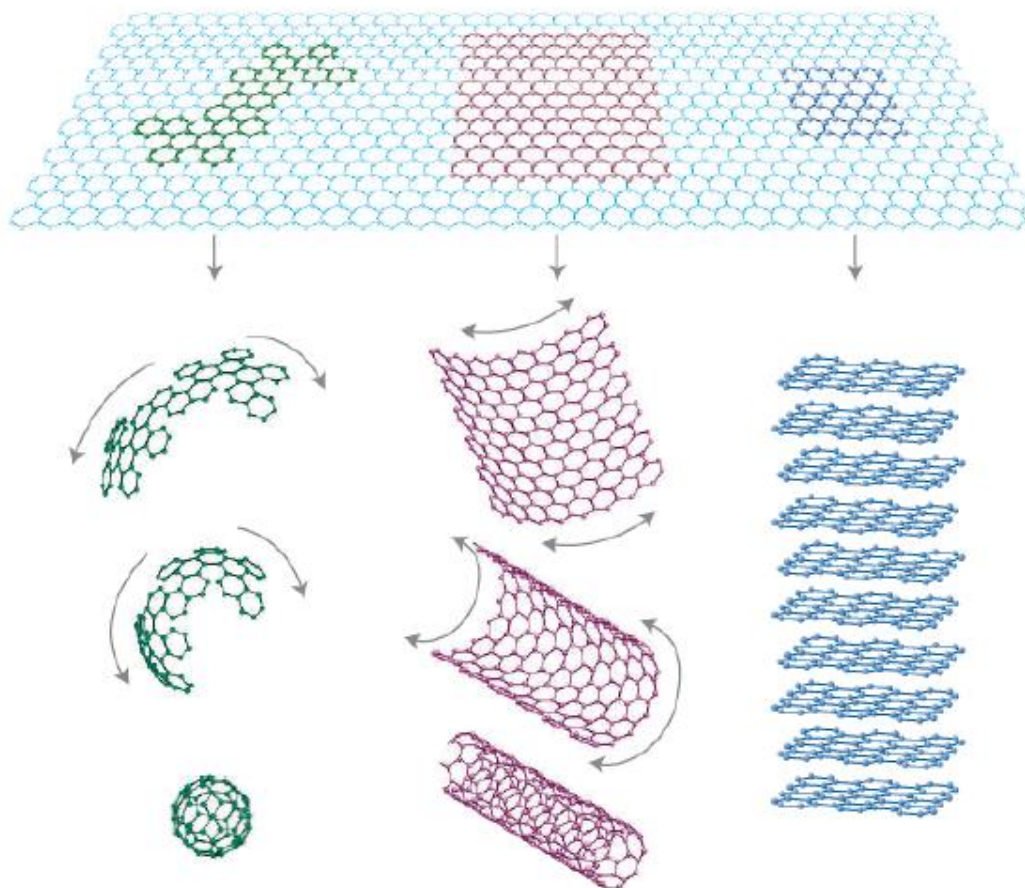
1.8 Introduction to Graphene

Graphite is a structure composed of carbon planes, with a separation of 0.335 nm between each other and arranged in a honeycomb net form (Pandit et al., 2018). A single atomic layer isolated from graphite that is composed of sp²-hybridized carbon atoms in a hexagonal crystal structure is called graphene (Singh et al., 2017).

Graphene, by definition, is a two-dimensional (2D) material with a Carbon-carbon distance of about 0.142 nm. It is considered as the primary material of all other graphitic carbon allotropes of different dimensionality (Fig. 2) (Kim et al., 2010).

For example, figure 2 shows how the graphene structure can be stacked to form 3-D-graphite, rolled to form 1-D-nanotubes, and wrapped to form 0-D-fullerenes (Ghuge et al., 2017).

Figure 2. The 2D graphene is the building block of carbon materials of all dimensionalities: 0D,1D, and 3D .



Source: (Ghuge et al., 2017).

1.9 Graphene Properties

Graphene is extensively investigated as novel material because of its distinctive physical and chemical properties applicable in several fields such as medicine, electronics, biotechnology, and biomedicine. In particular, graphene-based materials has provided several benefits in the evolution of new implants and biomedical devices serving as a coating biomaterial.

A graphene-based material must keep specific characteristics to be considered optimal; it must be flexible, resistant, antibacterial, non-toxic to human cells, and act as a good conductor. Also,

graphene seems to be an ideal candidate for implant surface coating for biomedical implants since it is chemically inert, atomically smooth, and highly durable.

1.9.1 Physical and mechanical properties

Graphene exhibits exceptional physical and mechanical properties that make graphene the strongest, attractive, and multifunctional material of the world.

Graphene-based materials are capable of combining different properties like thermal conductivity (5000 W/mK), the high electron mobility in room temperature (250,000 cm²/Vs), and good electrical conductivity to act as a superconductor, and as a field electric transistor in electromechanical systems. The stiffness, strength and toughness, intrinsic mechanical properties of graphene, are being studied by academia and industry due to its importance in the production of graphene-based materials. These exceptional mechanical properties are due to the stability of the sp² bonds that form a hexagonal lattice and oppose a variety of in-plane deformations (Papageorgiou et al., 2017).

Besides, graphene has Young's modulus of 1100 GPa, the fracture strength of 125 GPa, and a surface area that can reach 2630 m²/g, making it a resistant, flexible, and durable material (Yao & Fan, 2019). Table 2 describes the unique physical and mechanical properties of graphene as materials.

Table 2. Unique properties of Graphene as materials

Properties	Values
Charge carrier mobility (Papageorgiou et al., 2017)	250 000 cm ² /Vs
Thermal conductivity (Papageorgiou et al., 2017)	5000 W/mK

Specific surface area (Yao & Fan, 2019)	2630 m ² /g
Young's modulus (Yao & Fan, 2019)	1 TPa
Tensile strength (Yao & Fan, 2019)	1100 GPa
Bandgap (Merici et al., 2008)	<i>Zero</i>

1.9.2 Biological Properties

The interaction between the biological components (tissue, cells, and proteins) and graphene-based materials is a key issue for biomedical applications. Three aspects of the graphene-based layers used in biomedical devices dictate the suitability of the material: the thickness, the lateral extent, and the surface functionalization of graphene. Well-controlled those aspects the graphene-based materials could be beneficial, facilitating the intracellular transport of therapeutic or diagnostic agents, or providing antimicrobial shielding and even enhancing the cell growth, proliferation, and growth. (Kostarelos & Novoselov, 2014).

The Graphene-based materials are used as a substrate to interact with cells and biomolecules and enhance the compatibility, selectivity, and solubility of a biological system. Then, the graphene-based materials, for their beneficial properties, are widely used for biomedical applications such as scaffolds for mammalian cell culture, bone and teeth implantation, antibacterial materials, and others (Priyadarsini, Mohanty, Mukherjee, Basu, & Mishra, 2018).

2. Problem Statement

The constant increase in rheumatic diseases linked to aging, among which are osteoarthritis, rheumatoid arthritis, and osteoporosis, has become a problem of social relevance in both developed and developing countries. Among these diseases, osteoarthritis is considered the first cause of joint replacement because it causes pain and disability in older adults (Nielsen et al., 2017).

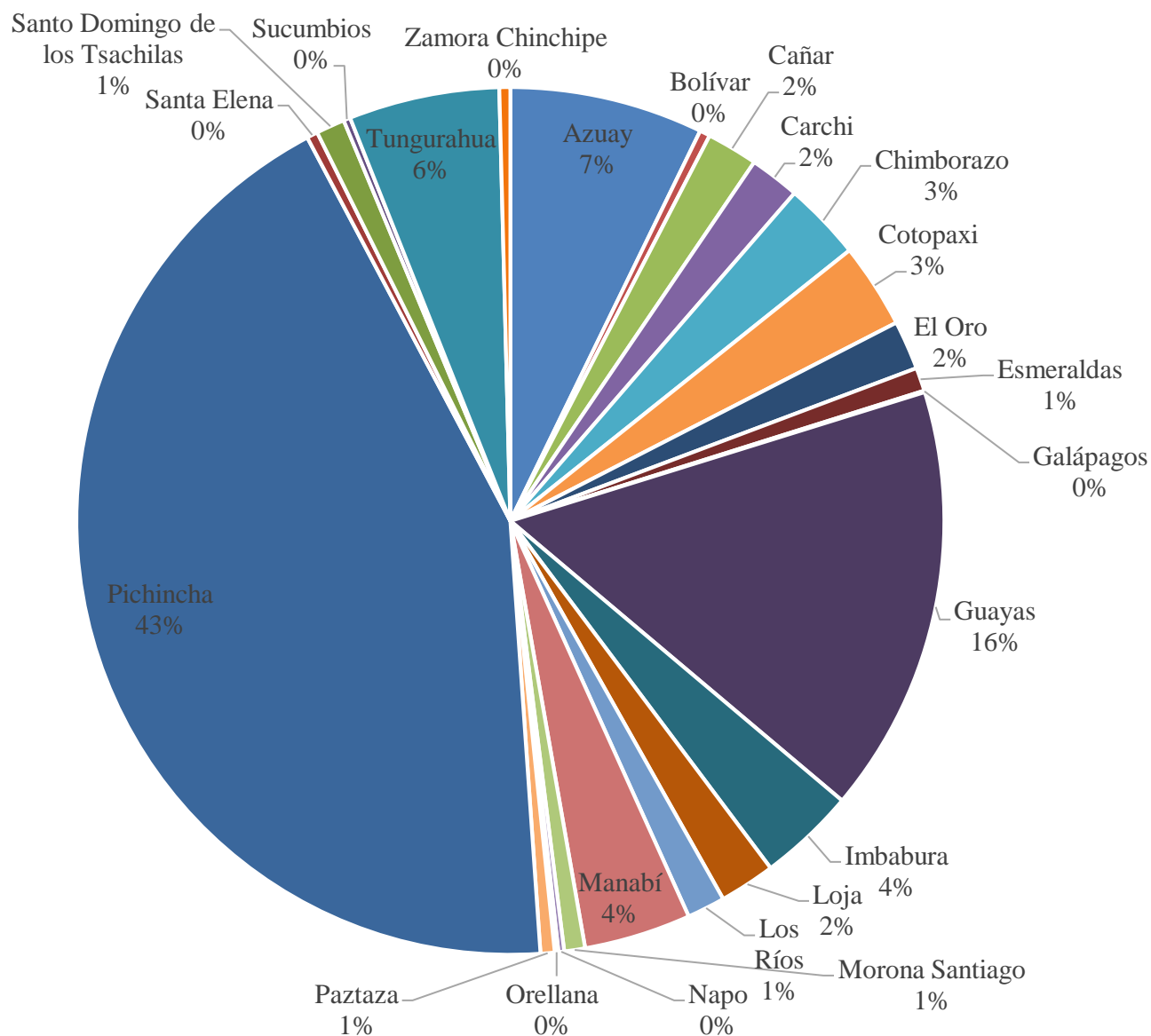
Specialists in orthopedics and biomedical engineering and materials have developed good quality joint prostheses with high success rates to improve the quality of life of people who must undergo surgery. However, joint replacement surgery is not without complications, considering the infection of the prosthetic material the most serious of all.

Therefore, it is crucial to develop new methods of disinfection and infection control that combat the formation of prosthetic biofilm and bacterial adhesion.

2.1 Infection associated with prosthetic joints in Ecuador

Ecuador does not have an official registry of arthroplasties, but official data from the INEC (National Institute of Statistics and Census) report cases of osteoarthritis (OA), the leading cause of joint replacement, within the 298 morbidity groups in the population. The increase in hospital discharges due to this pathology is evident, in the projections corresponding to the 2010-2020 period carried out by the INEC an average of 5154 cases of osteoarthritis is registered per year, an amount that is continuously increasing. The most vulnerable group to this pathology in Ecuador is the female one, with an approximate number of 3096 cases of osteoarthritis hospitalization per year. Also, a lethality rate of 0.27 has been recorded for every 100 hospital admissions for osteoarthritis. Most examples are with predominance in people over 65 years of age, but with a considerable number of cases distributed from 20 years of age (INEC, 2013).

Graph 1 shows a more detailed study of the incidence of osteoarthritis in Ecuador at the provincial level. Pichincha and Guayas have the highest rates of osteoarthritis incidence in the country. At a local level, a study conducted to determine the prevalence of early complications in patients undergoing arthroplasties at the Eugenio Espejo hospital in the city of Quito registered 16.6% of complications in knee arthroplasty, 34.7% were early complications, with infection prevailing (Torres & Enrique, 2018). Besides, an incidence of 2.27% is reported, data similar to international (Cañizares & Uquillas, 2015).

Graph 1. Incidence of Osteoarthritis in Ecuador

On the other hand, a study conducted at the Alcivar hospital in the city of Guayaquil found a global infection rate of 1.34% (Cobo, 2016).

The final stage of osteoarthritis is characterized by severe pain, disability, and joint deformity. The arthroplasty is the only effective treatment for osteoarthritis. It is inferred that the demand for joint replacement surgeries in Ecuador is also increasing, as the risk of getting a periprosthetic

infection. However, there are no specific data of periprosthetic disease, so there are no formal data at the national level of this pathology.

3. Hypothesis, General and Specific Objectives

3.1 Hypothesis

Graphene-based thin films can be a suitable biomaterial for killing bacteria due to their physicochemical properties. These thin-films could exhibit conductivity characteristics needed to apply variable frequency through the films and create an electromagnetic field that affects the polar parts of bacteria to avoid the prosthetic biofilm.

3.2 General Objective

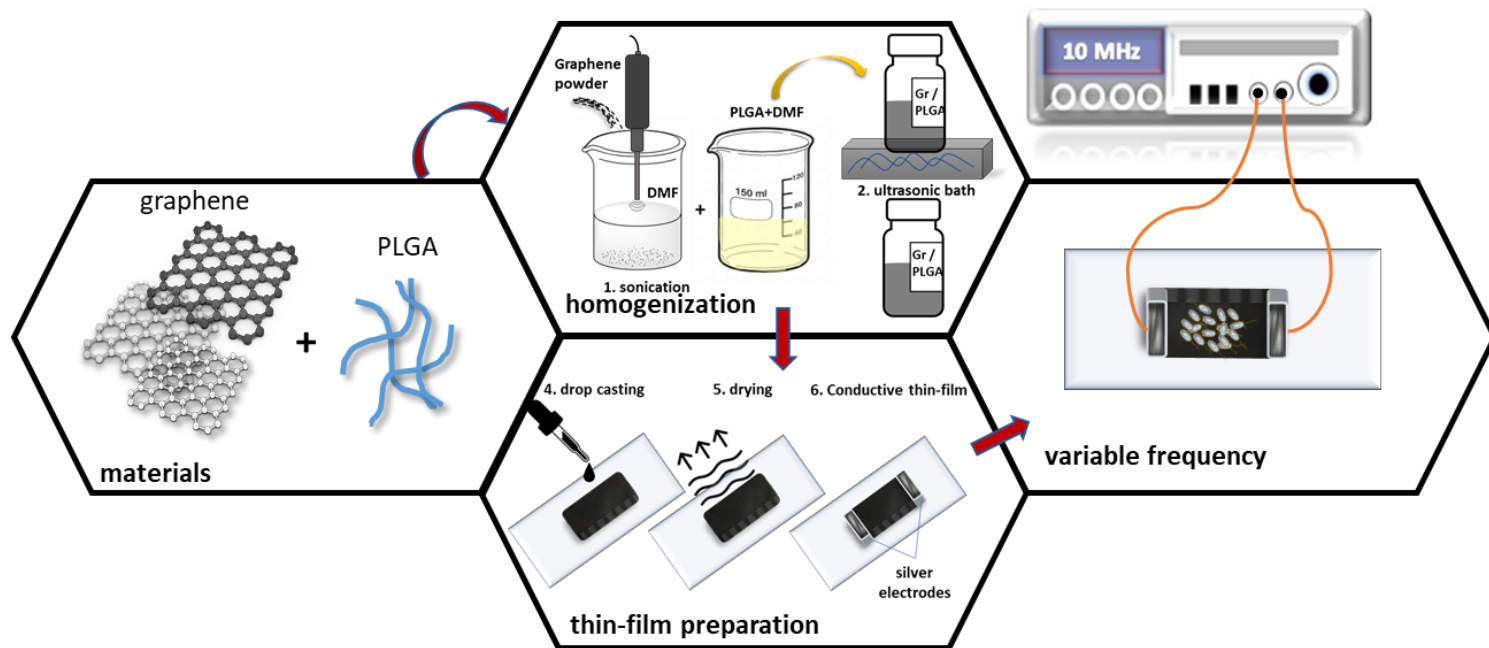
Prepare conductive films based on graphene to monitor and prevent the bacterial fouling on a surface and exerts antimicrobial action applying variable frequencies.

3.3 Specific Objectives

- Homogenize graphene nanoparticles through ultrasound using DMF.
- Add the PLGA copolymer to the sample and homogenize through the ultrasonic bath.
- Obtain thin layers of graphene by drop-casting by evaporating the solvent.
- Perform the physical-chemical characterization of the graphene-based thin layers to verify their conductive and surface properties.
- Integrate silver electrodes into thin sheets of graphene to create an electromagnetic field by applying variable frequency across the layers.
- Perform a circuit that allows direct connection of the graphene conductive layers to the frequency generator.

- Test the antibacterial capacity of the treatment based on variable frequency application on the thin layers of graphene (conductive) with gram-negative E. coli bacteria of strain TG1.

Scheme 1. Flow-chart of the objectives of this investigation



4. Methodology

4.1 Materials

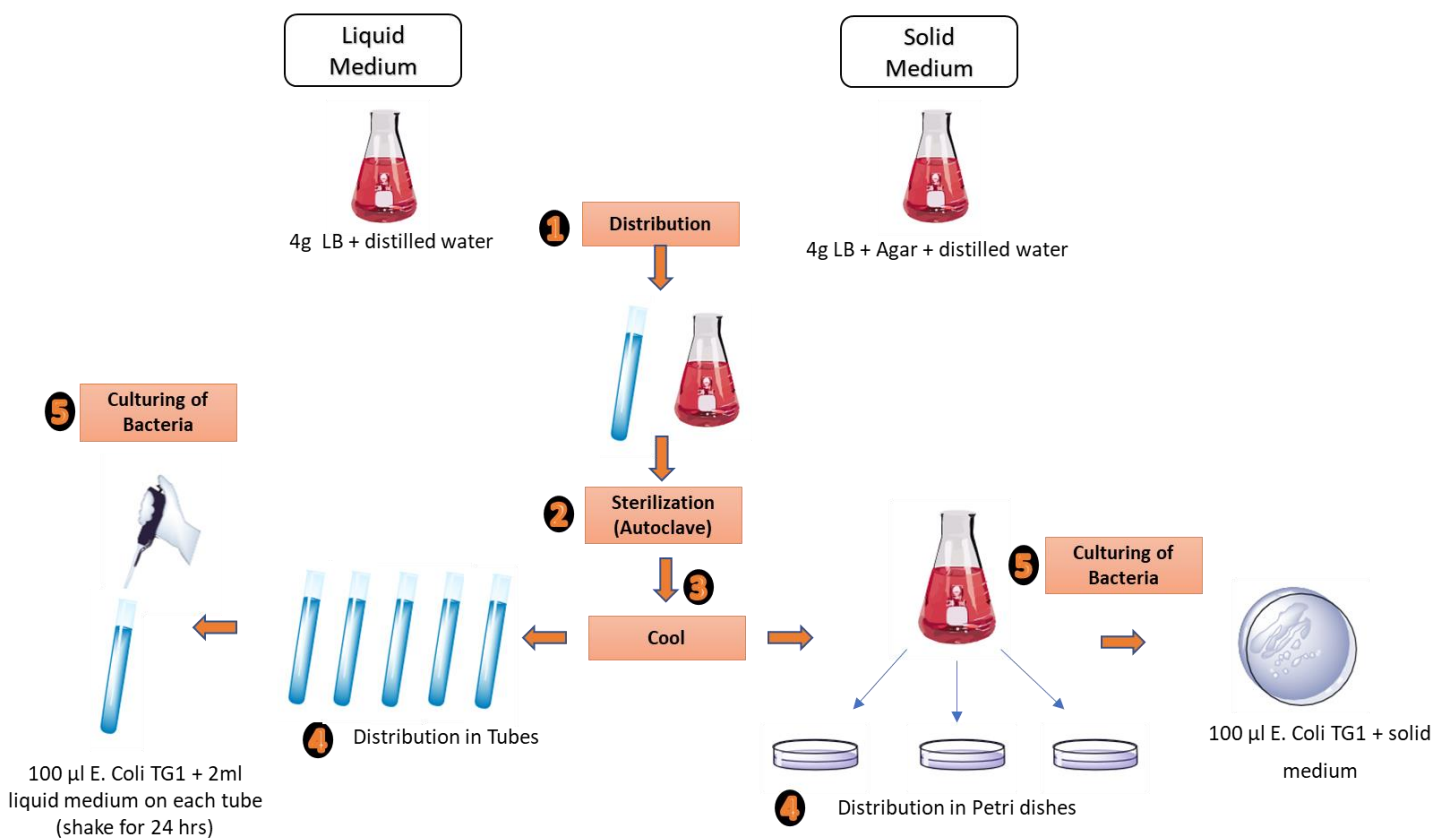
Poly (lactic-co-glycolic acid) (PLGA 2%) monomer ratio of lactide to glycolide: 85/15, CAS number: 26780-50-7, average molecular weight: 20,000 g/mol, N,N-Dimethylformamide (DMF), CAS number: 68-12-2, molecular weight: 73.09 g/mol, were acquired from Sigma-Aldrich. Conductive Silver paint was acquired from RS components (UK). Luria-Bertani broth Base (LB), (Lennox L Broth Base) containing tryptone, yeast extract, and sodium chloride (NaCl), CAT number: 12780-052 and LB Agar, powder (Lennox L Agar), CAT number: 22700-025, were supplied by Invitrogen, Thermo Fisher Scientific. Highly conductive Graphene Nanoplatelets

(GrFs) was supplied by Thomas Swan & Co. Ltd. (Product Ref: SP3073P) and fabricated by the solvent exfoliation route from graphite. The particle size ranged from 0.5 μm to 2.0 μm and is mainly composed of few-layer graphene flakes with an average of 5-7 atomic layers. This production method does not involve any aggressive intercalation or oxidative chemistry, providing non-oxidized and defect-free graphene powder. Typical Sheet Resistance is $10 (\pm 5) \Omega/\square$ for a 25m film.

4.2 Culture Medium Preparation

The culture medium is full of nutrients, growth factors, and other components that create optimal conditions for the development of microorganisms. To maintain *E. coli* TG1 bacteria and to observe colony formation, Luria Bertani Broth Base (LB) (4g) is used for liquid culture medium, and LB Agar (8g) is used for solid culture medium. To this solution is added 200ml of distilled water, respectively, for each type of crop. The dissolutions are autoclaved to 121°C , to homogenize and sterilize the culture media.

Scheme 2. Preparation of solid and liquid culture medium and E. Coli bacteria incubation



As can be seen in scheme 2, the development of the culture media is based on three simple steps (distribution, sterilization, and cooling).

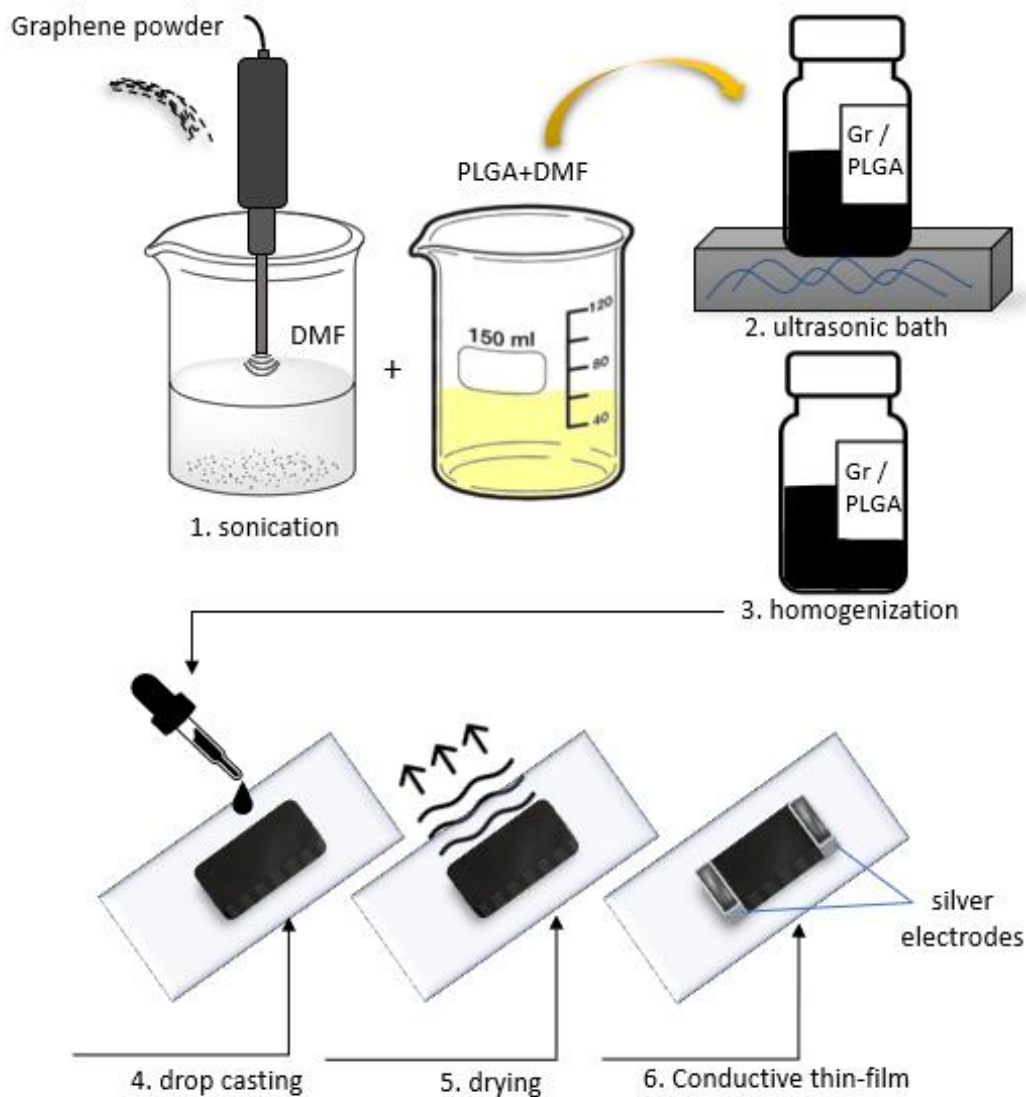
4.3 Bacteria Preparation

Escherichia Coli strain TG1 (E. Coli TG1) was supplied by Vispo N. (Yachay Tech University). A culture with 2mL of Luria Bertani (LB), the rich medium of aqueous growth, and 100 μ l of Escherichia coli bacteria of strain TG1 (E. coli) were cultivated for 24 hours at 37 °C with shaking (scheme 2). The benefits of using microorganisms, such as Escherichia Coli, are the rapid growth rate and simple nutritional requirements. These properties allow E. Coli to grow in a minimal culture medium with glucose as a source of carbon, salts, and trace elements (Lodish et al., 2000).

4.4 Graphene Thin-films fabrication

Thin graphene conductive films were manufactured using homogeneous solutions of PLGA and Graphene as base materials. The preparation of graphene-based thin layers follows a two-step solution mixing protocol (scheme 3).

First, a 0.1 wt% graphene sample was prepared using 10ml of N.N-Dimethylformamide (DMF), an organic solvent, to form graphene dispersions with long-term stability, easy to handle and process (Paredes et al., 2008). The graphene suspension was homogenized by tip sonication with a SONOLUS mini20 sonicator equipped with a 2.5 mm microtip. The sonicator operates at 75kHz and 20W for 1-second pulses with ice around to avoid overheating the sample. The solution was sonicated for 60 minutes until a black mixture was obtained without apparent aggregates. Second, two wt% of poly (lactic-co-glycolic acid) PLGA was dissolved in 10ml of DMF. The mixture was stirred at room temperature in an ultrasonic bath sonicator until a light-yellow homogeneous mixture was obtained.

Scheme 3. Graphene Thin-films Preparation

Finally, thin conductive films based on macroscopic Graphene / PLGA were obtained by mixing at room temperature 9ml of the 0.1 wt% Graphene dispersion with 1ml of 2 wt% PLGA solution. The solution was poured into a 5 cm diameter Petri dish and allowed to evaporate for 48 hours at room temperature. A rectangular region of $10 \times 5 \text{ mm}^2$ was isolated in each film. Then

the edges were coated with a silver paste to create electrodes with surface conductivity and frequency measurement.

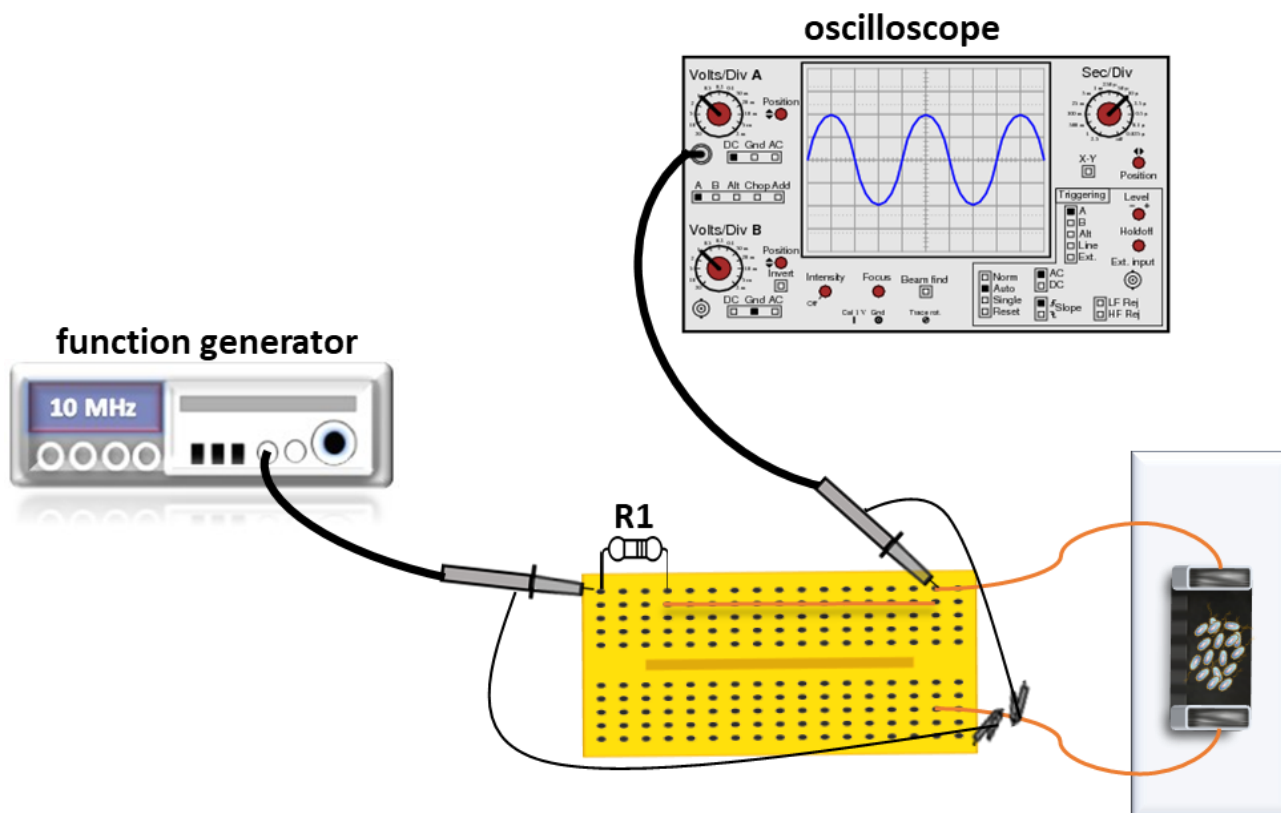
4.5 Graphene Thin-films Characterization

Several methods for characterizing graphene / PLGA-based thin layers were used to investigate and study the properties and characteristics of the material; the morphology and structure were examined by scanning electron microscopy (SEM), the cross-sectional structure was observed by transmission electron microscopy (TEM), the chemical composition was analyzed by X-ray diffraction (XRD), and Raman Spectroscopy studied the crystalline structures and the quality of the thin-films based on graphene.

4.6 Conductivity Experimental Setup

To send constant variable radiofrequency for 1 hour through the thin-films based on graphene, an electronic circuit was configured. This device allows monitoring the wave signals sent with an integrated oscilloscope to send constant variable radiofrequency for 1 hour through the thin-films. The circuit was armed with a high function generator resolution that uses technology to deliver an output signal in the range of 5MHz-15MHz with high precision and low distortion. The circuit connects directly to the graphene-based thin layers through silver electrodes that allow constant conductivity across the layers. Also, a current limiter (R1) was included, which will deliver the voltage source, regardless of the impedance of the load (scheme 4).

Scheme 4. Schematic configuration and main elements of the variable frequency experimental set up used to stimulate bacteria.



4.7 Effect of Electric field on Escherichia coli TG1 Growth

The *E. coli* solution was diluted (1: 100 v / v) in 900 ml of the new LB liquid culture medium to restart the cell cycle. After 1 hour of incubation at room temperature, the control cells (without treatment) were synchronized in the logarithmic phase of the growth curve, with an optical density at 600 nm of 0.05-0.005, with constant growth, where the cells are dividing and result in metabolic activity. To test the bactericidal properties of the fabricated circuit, 100 μ l of *E. coli* culture was placed on thin layers of graphene of dimension (3 * 1 cm), and the set-up was put to work. The

silver electrodes were far from the culture to avoid electrokinetic interference. Variable radiofrequency was applied to the 5MHz-15MHz range for 1 hour, to create an electromagnetic field on the conductive layers and affect the polarity of microorganisms. The optical density at 600 nm of the radiofrequency treated culture was measured, obtaining values of 0.04-0.003. Control and radiofrequency treatment cultures were maintained for 12 hours at room temperature. Serial dilutions of the culture were made at 1 and 12 hours, and 100 µl of each dilution were grown in sterile LB agar, solid culture medium and incubated at 37 ° C. After 15 hours, the number of colonies on each plate was determined to obtain the bacterial survival concentration. Cell log N was calculated with the determination of Colony Forming Units (CFU), using the formula:

$$\frac{CFU}{ml} = \frac{No. of Colonies \times dilution factor}{Volume of the culture spread}$$

4.8 Structural and morphological Characterization of Escherichia Coli TG1/Graphene/PLGA thin-films

The morphological changes of the bacteria after their death due to the variable radiofrequency treatment applied were studied using scanning electron microscopy (SEM). Nanoparticles' structure and film surfaces were assessed by using a Field-Emission Scanning Electron Microscope (Tescan Mira3). Samples were placed on aluminum sample-holders and then metalized for 60 seconds with a 20 nm thick gold layer (Sputter Coating Quorum Q105R) before observation. The operation voltage was settled to 10 kV (Arroyo Rodriguez, 2018).

4.9 Statistical Test

To statistically analyze the results, a one-way analysis of variance (ANOVA) was performed. The absorbance of the observations was set as the dependent or response variable, and the different

treatments (0MHz, 5MHz, 10MHz, 15MHz) were set as levels of the factor variable. The null hypothesis was set as: The mean absorbance stays the same in observations under different treatments, and therefore our alternative hypothesis was: The mean absorbance of at least one group of views is different from the others. The ANOVA test was carried out with the help of the version 3.4.4 of the R programming language (R Core Team, 2018). The source code and the data required as input can be found in Annex C.

5. Results

5.1. Graphene/PLGA Thin-films Characterization

SEM

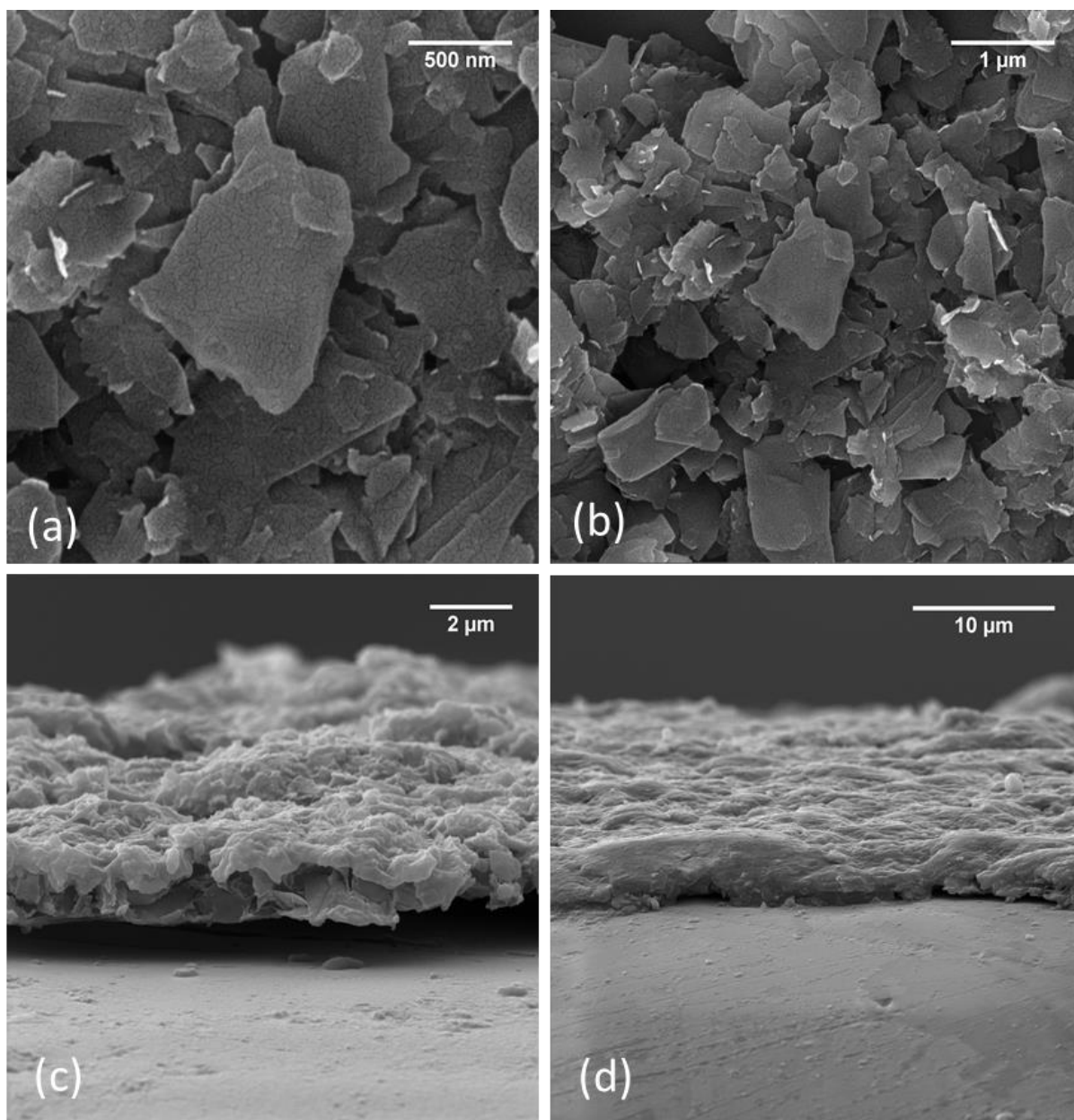
Nanoparticles' structure and film surfaces were assessed by using a Field-Emission Scanning Electron Microscope (Tescan Mira3) by Alexis Debut (Universidad de las Fuerzas Armadas ESPE). Samples were placed on aluminum sample-holders and then metalized for 60 seconds with a 20 nm thick gold layer (Sputter Coating Quorum Q105R) before the observation. The operation voltage was settled to 10 kV to avoid the damage of the samples.

A lateral SEM analysis analyzed the thickness of the thin layers of graphene, and an average was calculated using the tools of the ImageJ software. A depth of 2 μm to 5 μm was obtained in each thin layer.

On the other hand, the horizontal view shows the accumulation and stacking of a graphene multilayer with a wrinkled and bulky topology. Where almost all the graphene flakes had a dimension between 0.320 μm and 1.094 μm , it is believed that the roughness of the nanoscale surface can play an essential role in improving mechanical interlocking and load transfer through the multilayer (Shahil & Balandin, 2012).

The figure 3 (a, b) shows the irregularities in the thin-layers and the stacking structures formed in the multilayer based on graphene/PLGA in different scales 500 nm and 1 μ m respectively and, (c, d) shows the thickness of the multilayer on a glass substrate in different scales 2 μ m and 10 μ m respectively.

Figure 3. SEM morphologies of Thin-films based on Graphene



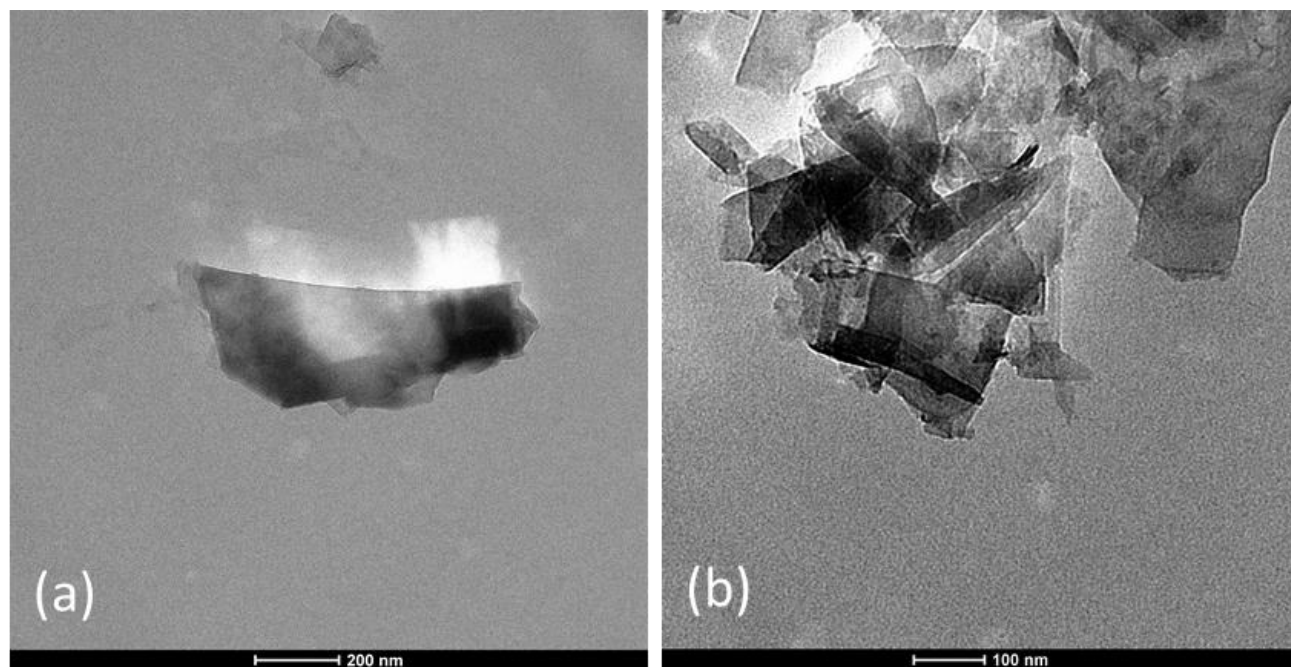
TEM

TEM analysis was performed using an analytical TEM brand FEI model Tecnai G20 TWIN SPIRIT at ESPE. The procedure voltage was settled at 200 kV to avoid the damage of the samples. The cross-sectional TEM sample was prepared using the conventional focused ion beam method.

TEM observation can identify the stacking structures and analyze the detailed cross-sectional structure of the graphene thin-films based on the crystallinity of the material, which is a typical thin transparent film for graphene (Murata et al., 2019).

In figure 4 are shown isolated small dimensions of the graphene multilayer analyzed by TEM. The spectra show a few Graphene layers flake with a lateral size of 90-250 nm. Fig. 4 (a) shows a flake conformed by 3-4 coats of graphene seen by color contrast. Most of the flakes are characterized by folded and wrinkled area, such as in Fig. 4 (b) that is composed by many and disordered layers, which may indicate that these flakes are formed by re-aggregation during deposition on the TEM grid (Yang et al., 2013).

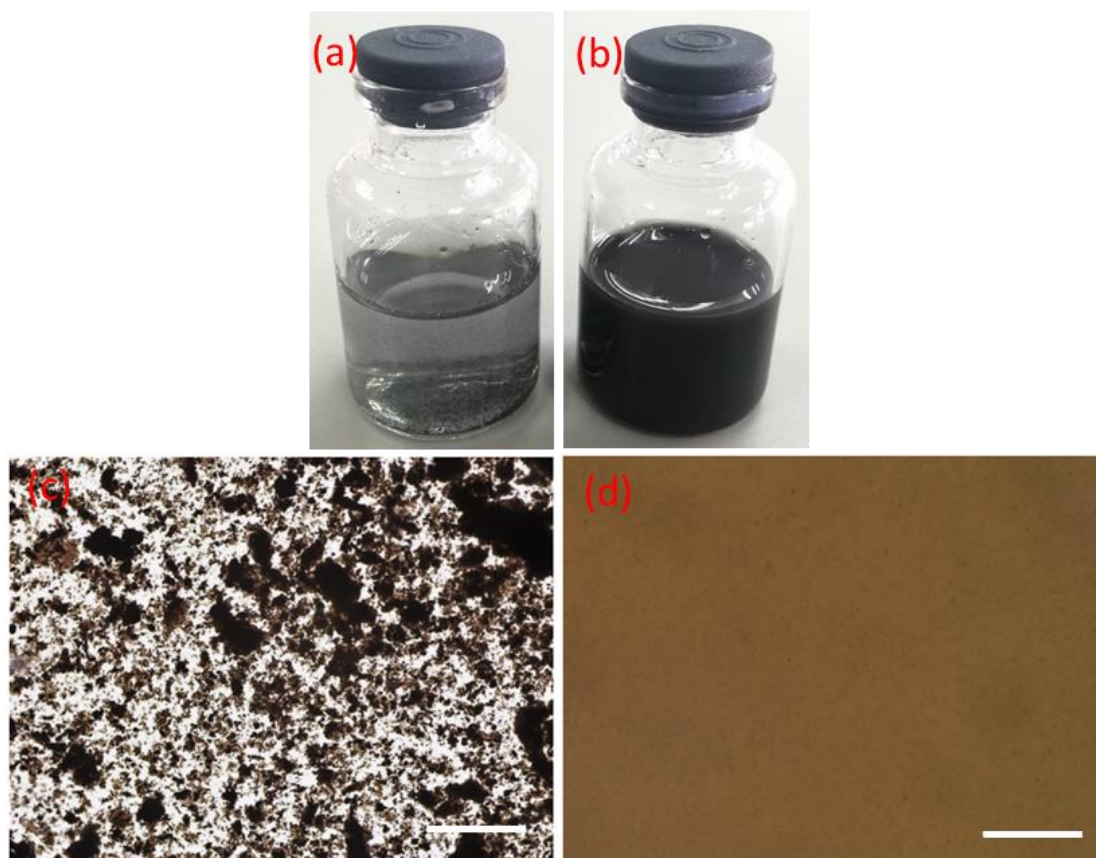
Figure 4. TEM cross-sectional structure of Thin-films based on Graphene



Optical Microscopy

Figure 5 shows the homogeneity and stability that was evaluated on a macroscopic scale, followed by observations with non-polarized optical microscopy to verify the dispersion of the carbon nanoparticles on a microscopic level. Photographs of vials containing 10 mL of aqueous solutions of graphene Elicarb (Gr-e) 0.1 wt% and 1mL PLGA 2%. (a) solution before sonication, (b) solution after 30 min of tip sonication. Typical brightfield optical micrographs of Graphene Elicarb dissolutions (c) before sonication (d) after sonication. The uniformity of the picture reveals the absence of particles or aggregates with a dimension that exceeds a micrometer, the standard order of the optical microscope resolution. Scale bar 50 μm .

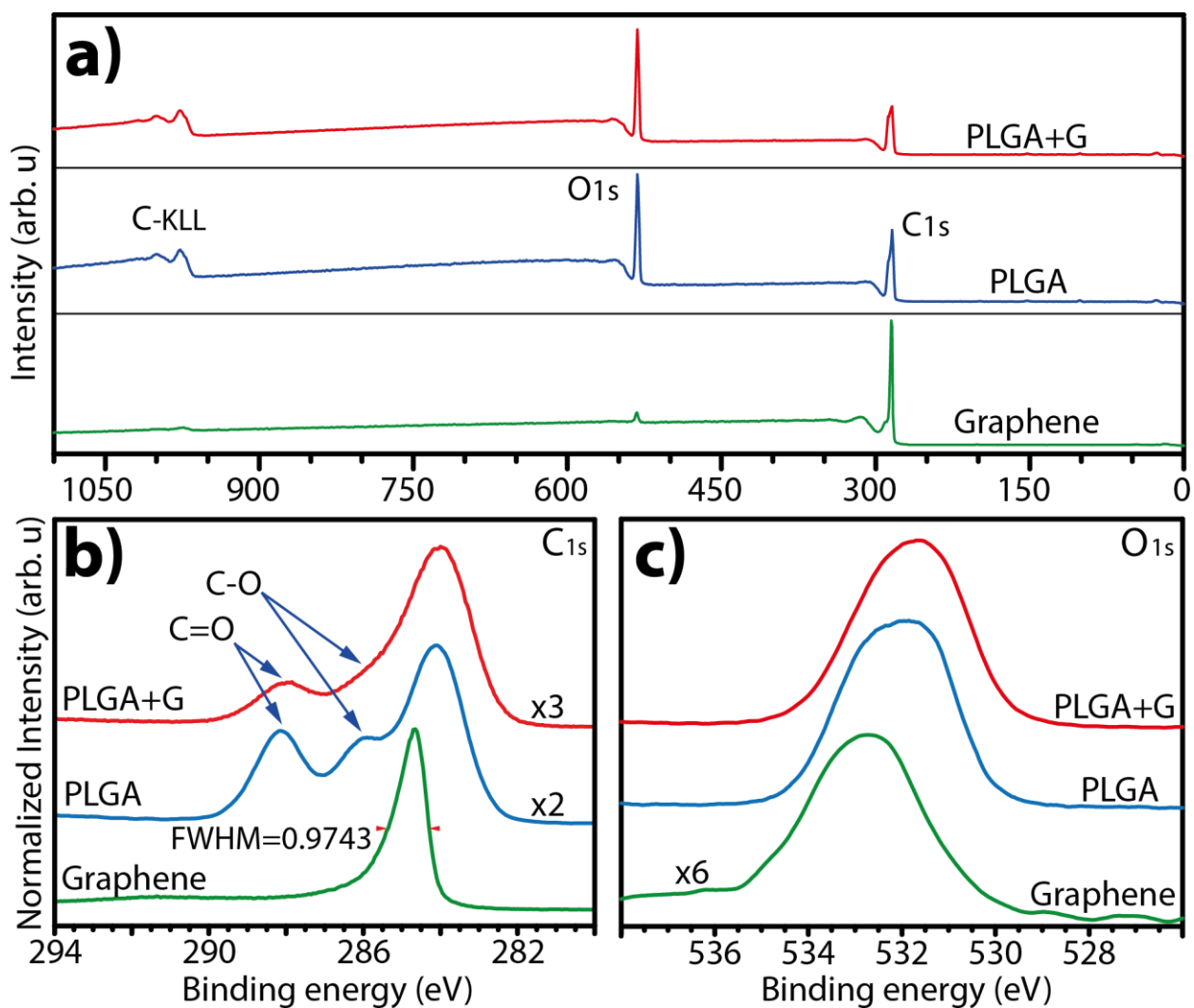
Figure 5. Graphene dispersions



XPS

Binding chemistry environment characterization was performed by X-ray Photoelectron Spectroscopy (XPS), using a VersaProbe III from Physical Electronics, equipped with a 180 hemispherical electron energy analyzer and excited by a monochromatized Al K α source with an energy 1486.6 eV operated with an energy bandpass 55 eV. The analysis spot had a diameter of 100 μm , setting a 45° detection angle to the substrate surface.

Graph 2. XPS spectra for graphene powder (Gr), PLGA powder and, a PLGA/Gr thin film.



Graph 2 a) reports the C 1s, O 1s and, C-KLL spectra from the carbon and oxygen atoms of the PLGA, Graphene, and PLGA/Graphene films at the surface stage. The fitted C 1s spectrum of the PLGA and PLGA/Graphene sample reveals the presence of C-C, -C=O and, -C-O bonds at 286 eV, 288 eV, and 286 eV, respectively. Meanwhile, the O 1s spectrum can be fitted with a band for each sample at; 532.5 eV (Graphene) attributed to OH⁻ species derived from a possible decomposition process as the result of a specific enrichment in the oxygen of the surface that is also evidenced in the Graphene/PLGA sample C 1s spectrum and, 531.7 eV (PLGA and PLGA/Graphene) attributed to O=C-, chemical species (López-Santos et al., 2015; Shin et al., 2012).

Raman

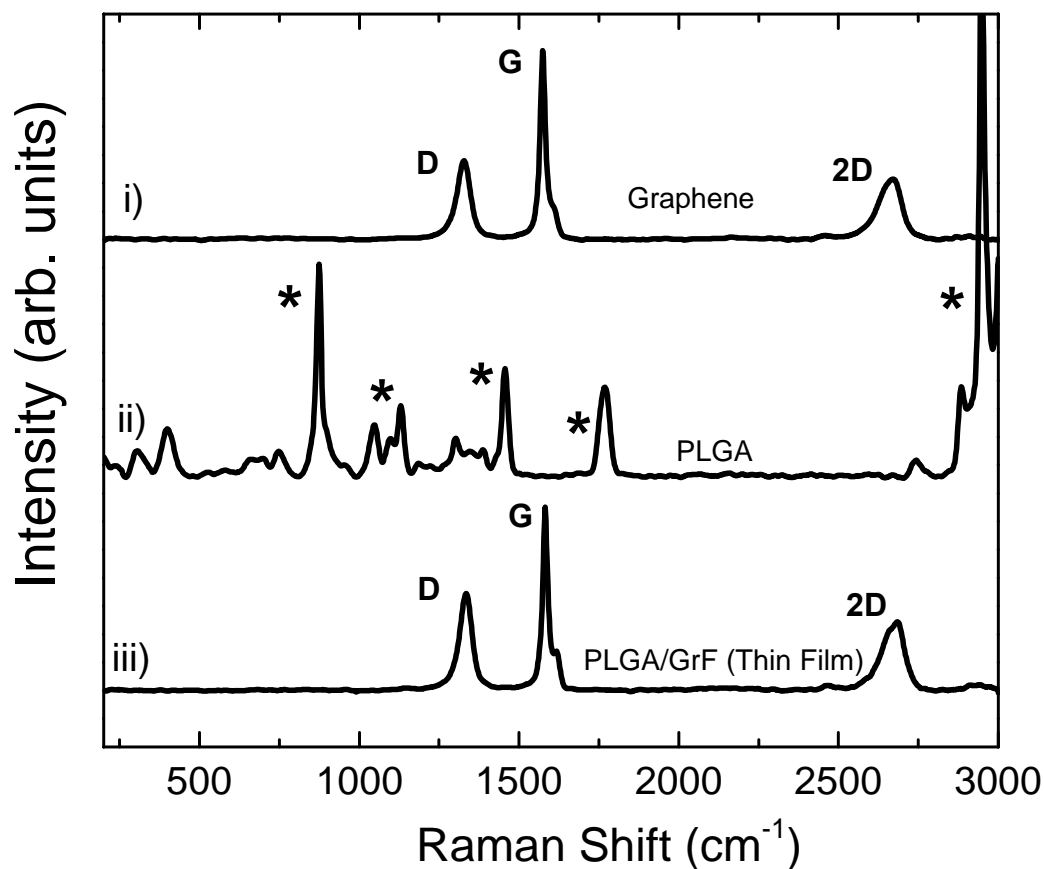
Raman spectroscopy measurements were carried out using a Horiba LabRAM HR evolution Raman spectrometer coupled with a CCD camera and excited by a solid-state red laser line ($\lambda_{\text{exc}} = 633 \text{ nm}$) and equipped with a microscope configuration. Our measurements were performed at room temperature, using a 100 \times objective lens with a long working distance, a laser spot size of 0.5 μm , and a spectral resolution of 0.35 cm^{-1} . The power laser was below 50 mW to avoid sample-overheating effects. The spectrometer was calibrated using a silicon wafer with a typical Raman feature at 521 cm^{-1} . Spectra were recorded in the 200–3000 cm^{-1} region with an 1800 grooves/mm grating. Usual recording time was between 10 and 1000 s depending on the intensity of the signal, and two accumulations per spectrum segment were averaged.

The Raman spectrum provides crucial information about the crystalline structures of the matrix and the presence of defects in the carbonaceous phases. Besides, concerning graphene, Raman

spectroscopy guarantees the quality assessment of the graphene phase during the different stages of nanocomposites processing (Lazzeri, 2012).

Graph 3 shows the Raman spectra in the range of 200-300 cm^{-1} for i) a graphene flakes powder, ii) a PLGA, and iii) a PLGA/Graphene thin film. For graphene powder, we observe a flat spectrum with a D-band or a defect band around 1350 cm^{-1} that is related to suspensions with hydrosoluble polymers (Torres-Canas et al., 2015). On the other hand, the G-band or Graphitic band corresponds to carbon-carbon in-plane stretching in graphitic materials. It is also observed the D'-band or Gs-band around 1620 cm^{-1} , corresponding to the elastic backscattering that makes recombination possible and its intensity scales proportionally as the sources of impurities increases, due to an enhancement of the backscattering (Heller et al., 2016).

Graph 3. Raman spectra for (i) a graphene powder (Gr), (ii) a PLGA powder, and (iii) a PLGA/Gr thin film.



Finally, as expected in Graphene samples, a vibrational band at 2700 cm^{-1} is observed. Conversely, the spectrum for PLGA (Figure 3 (ii)) exhibits characteristic features with very distinct groups peaking at 880 , 1090 , 1130 , 1300 , 1450 , and 1765 and 3000 cm^{-1} . The central peak at 880 cm^{-1} is associated with stretching C-COO, the 1450 cm^{-1} is attributed to CH_3 antisymmetric deformation, while the peak located around 1765 cm^{-1} is due mainly to C=O stretching. Finally, the prominent band observed at 3000 cm^{-1} is attributable to CH_3 and CH_2 antisymmetric stretching (Peleias Junior et al., 2015).

As expected, for PLGA/Graphene thin films (Graph 3 (iii)), the spectrum shows Raman fingerprints for Graphene, i.e., D, G, and 2D bands, while the Raman features from PLGA are no longer observed. It is in concordance with literature because in graphitic materials, the Raman process is resonant, and so their signal is much more intense than the non-resonant signal from PLGA. These findings indicate that the structure of the Graphene and PLGA is conserved in the final nanocomposite (Esquivias et al., 2019).

5.2. Antibacterial Test

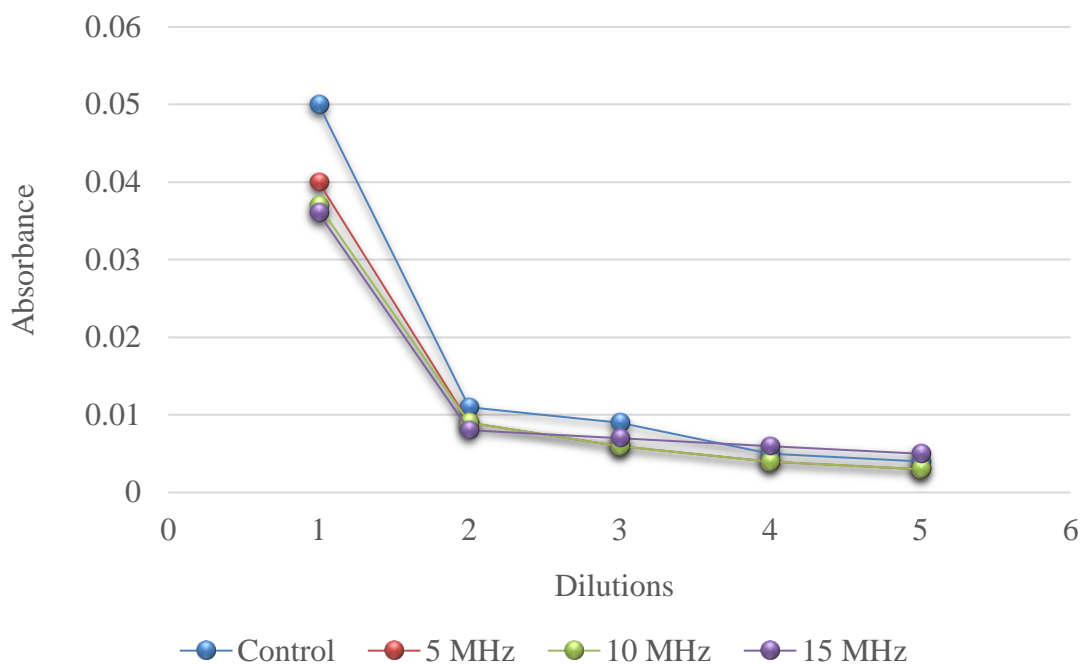
At basal conditions, the absorbance of the culture medium at 600 nm was 0.05 (Graph 4). After applying a radiofrequency of 5MHz, the absorbance decreased by 20%, which is a significant value. At 10MHz, the absorbance has been reduced another 6% concerning control conditions. In the end, a 15MHz radiofrequency was applied to the culture, obtaining an absorbance value of 0.036, which represents a 28% absorbance reduction for the control. The absorbance was measured at five dilutions, and the optical density resulted in lower values as higher radiofrequency applied in all of the dilutions.

Table 3. Absorbance values of the culture medium at 600 nm 1-hour after the RF treatment

Dilutions	Control	5MHz	10MHz	15MHz
1	0.05	0.04	0.037	0.036
2	0.011	0.009	0.009	0.008
3	0.009	0.006	0.006	0.007
4	0.005	0.004	0.004	0.006

5	0.004	0.003	0.003	0.005
---	-------	-------	-------	-------

Graph 4. Absorbance measurement of the culture medium at 600 nm 1-hour after the RF treatment

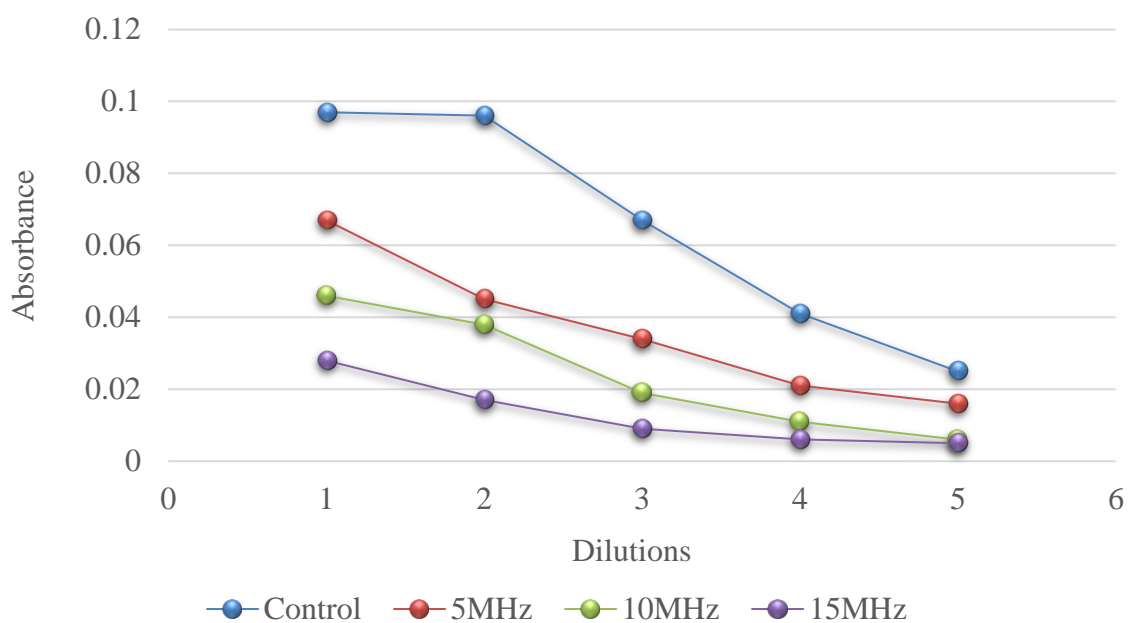


After 12 hours of incubation at room temperature, the optical absorbance of the control medium is 0.097 (Graph 5). Graph 5 shows an increase of 94% regarding the first measurement, and this means that the number of cells has doubled. On the other hand, the absorbance of the culture medium treated with 5MHz of radiofrequency has increased by 67%, at 10MHz has increased 24%, and at 15MHz, there is not an increase of absorbance. This last one has been reduced by 33% concerning initial measurement. Moreover, the optical absorbance values of the five dilutions follow the same pattern of cell number reduction.

Table 4. Absorbance values of the culture medium at 600 nm 12-hours after the RF treatment

Dilutions	Control	5MHz	10MHz	15MHz
1	0.097	0.067	0.046	0.028
2	0.096	0.045	0.038	0.017
3	0.067	0.034	0.019	0.009
4	0.041	0.021	0.011	0.006
5	0.025	0.016	0.006	0.005

Graph 5. Absorbance measurement of the culture medium at 600 nm 12-hours after the RF treatment



Bacteria counting

Colonies were counted using ImageJ software. The countable dilution is the dilution that gives 3 to 30 colonies per 10 μ l drop of sample dispensed. This rule is consistent with the SP method for

which one counts at the sample dilution containing 30 to 300 colonies per plate. The total count is scaled up, and the viable cell counts are expressed as CFUs per beaker volume (Herigstad et al., 2001). Table 5 shows the bacteria counting cultured after 1 hour of radiofrequency treatment, where only dilutions containing 30 to 300 colonies of bacteria per plate were considered (underlined in blue).

Table 5. Colony count of E. Coli TG1 per plate

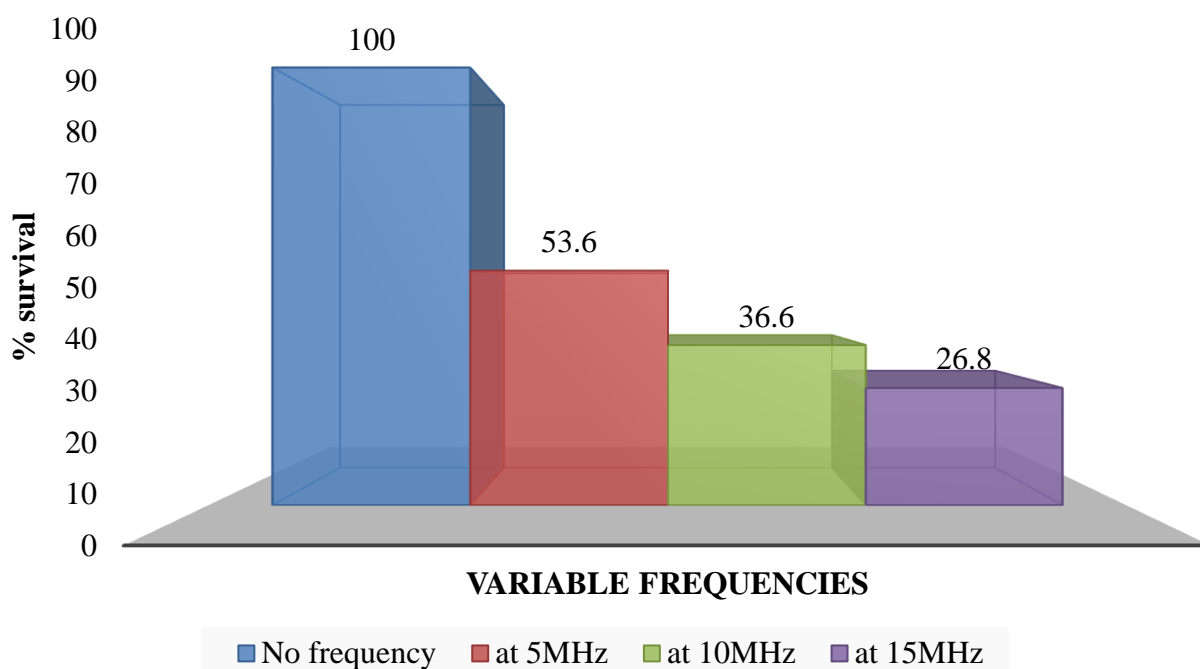
Dilutions	Control	5MHz	10MHz	15MHz
1	112000	60000	41000	30000
2	11200	6000	4100	3000
3	1120	600	410	300
4	112	60	41	30
5	11.2	6	4	3

Bacterial survival after 1-hour exposure to variable frequencies

The bacteria of the five dilutions treated with the three different radio-frequencies were cultured in solid LB agar and incubated at 37°C for 1 hour. The number of colonies in the resulted plates was calculated, giving as a result of a survival rate corresponding with the absorbance values obtained in the liquid culture media dilutions. The values of the survival rate of bacteria are shown in a bar graph (Graph 6). The control culture has a 100% survival rate, whereas the culture treated with 5, 10, and 15 MHz of radio-frequencies have a survival rate of 53.6%, 36.6%, and 26.8%, respectively.

Table 6. Bacteria survival Analysis

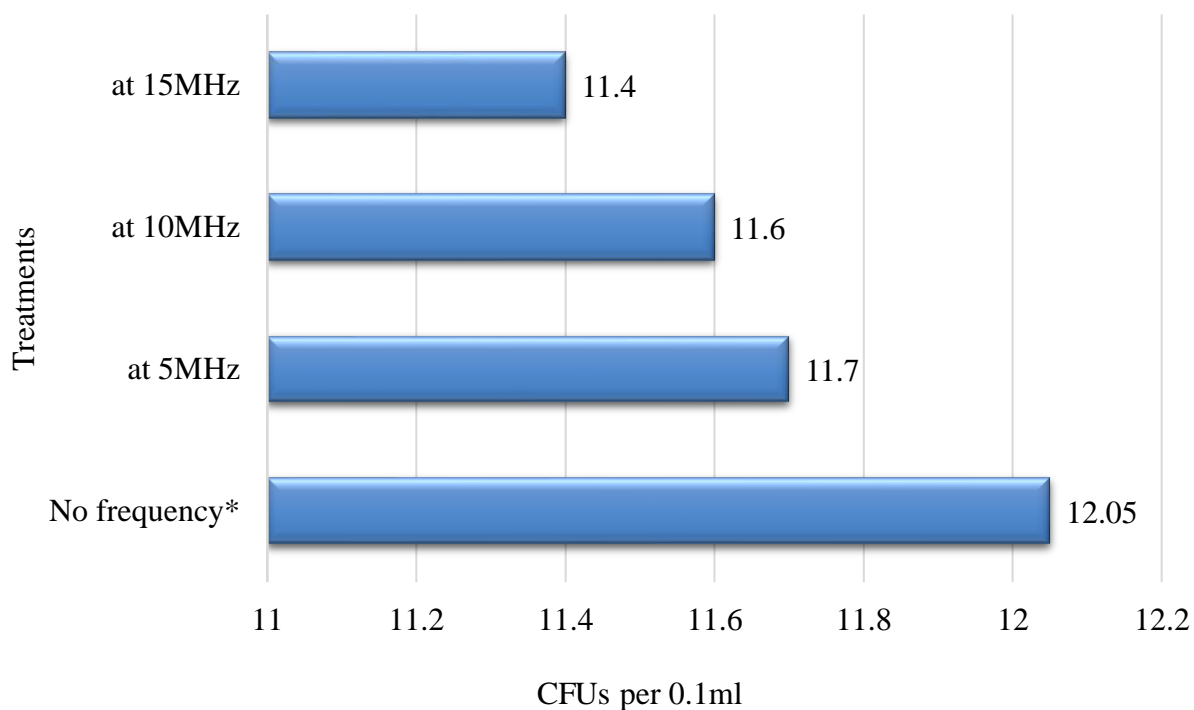
Treatments	No. of colonies	% survival
Control	112	100 %
5MHz	60	53.6 %
10MHz	41	36.6 %
15MHz	30	26.8 %

Graph 6. The survival rate of bacteria after the RF treatment at different frequency values

In Graph 7 are represented the calculated CFUs per 0.1mL of the volume of liquid culture. Accordingly, the CFUs are lower in the culture medium treated with 15MHz with 11.4 CFUs. The control medium was calculated to have 12.05 CFUs per 0.1mL, the medium treated with radio-frequencies of 5 and 10 MHz had 11.7 and 11.6 CFUs per 0.1mL, respectively.

Table 7. Colony Forming Units (CFUs) Values

Treatments	CFUs per 0.1mL
Control	12.05
5MHz	11.7
10MHz	11.6
15MHz	11.4

Graph 7. Measurement of the CFUs concerning the different radiofrequency treatments

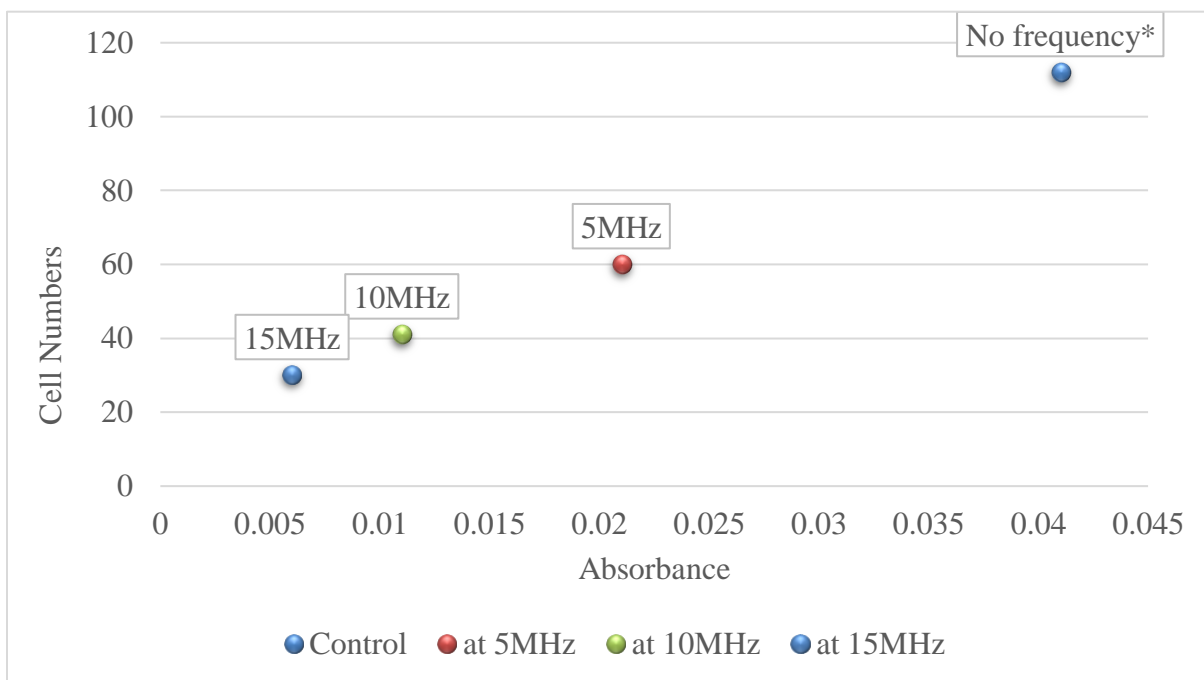
All of the measured values of absorbance, CFUs, and several colonies showed similar results. The number of cells is lower as the radiofrequency applied is higher (Graph 8). In this sense, the culture medium with no radiofrequency used has a higher number of cells, which is 112 giving an

optical absorbance of 0.041. At 5 MHz, the number of cells is 60, and the absorbance is 0.021. In the culture medium treated with 10 MHz, the absorbance measured was 0,011, and the cell number is 41. Finally, the higher radiofrequency applied in the culture medium was 15MHz, giving an absorbance of only 0,006, which represents 30 cells. It is essential to obtain colony cell numbers between the range of $300 < \text{cells} < 30$. Less than 30 may not be statistically significant, and 300 are too much to be counted on the plate. Table 8 shows the typical absorbance values according to dilution four cell numbers.

Table 8. Number of cell colonies and absorbance values

Parameters	Control	at 5MHz	at 10MHz	at 15MHz
Absorbance	0.041	0.021	0.011	0.006
Cell Numbers	112	60	41	30

Graph 8. Relationship between the number of cell colonies and absorbance values



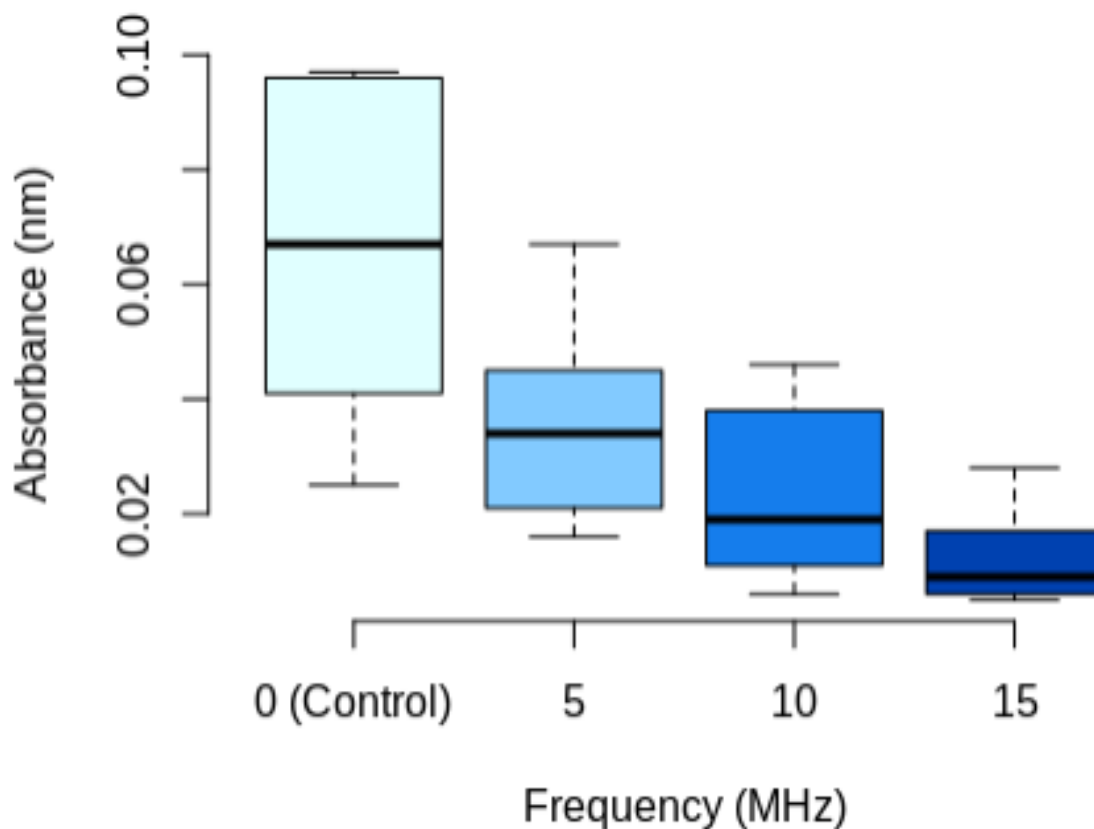
5.3. Statistical Analysis

First, mean absorbance and its standard deviation of the observations under different treatments was computed:

Table 9. Summary of statistical information concerning each group observations

Frequency	count	mean	sd
0 (Control)	5	0.065	0.0323
5	5	0.037	0.0204
10	5	0.024	0.0173
15	5	0.013	0.0096

To obtain an intuitive representation of the data, this information was plotted:

Graph 9. Average values for each treatment concerning their absorbance values

After developing the ANOVA test, the following results were obtained:

Table 10. Summary of the ANOVA test

Parameters	Df	Sum Sq	Mean Sq	F value	Pr(>F)
Frequency	3	0.007596	0.002532	5.473	0.0088
Residuals	16	0.007402	0.000463	-	-

Since the p-value was less than the significance level (0.05), the null hypothesis can be rejected, i.e., there exists a significant difference between some groups of observations. Furthermore, a pairwise-comparison between groups of observations was performed through the Tukey's range test:

Table 11. Summary of pairwise t-test comparison of observation

Frequency	diff	lower	upper	p adj
5-0(Control)	-0.029	-0.0675193	0.01031934	0.194339
10-0(Control)	-0.041	-0.0801193	-0.00228067	0.03614
15-0(Control)	-0.052	-0.0911193	-0.01328067	0.007135
10-5	-0.013	-0.0515193	0.02631934	0.791392

It can be seen from the output that there only exists a significant difference between the groups under the 10 MHz and 15 MHz treatment and the Control group. This suggests that there may exist a frequency threshold between 5MHz and 10MHz for the procedure to be effective.

It should be noted that to use the ANOVA test, regular distribution of factor levels, and constant variance between groups were assumed. Indeed, homogeneity of variances was verified through the Levene's test:

Table 12. Levene's Test for Homogeneity of Variance

Levene's Test for Homogeneity of Variance (center = median)		
Df	F value	Pr(>F)
3	2.1786	0.1304

A p-value greater than the significance level 0.05 indicates that there is no proof that there is a statistically significant difference between group variances. Similarly, the normal distribution of factor levels was verified using the Shapiro-Wilk test:

Table 13. Shapiro-Wilk normality test

Shapiro-Wilk normality test	
W = 0.96857	p-value = 0.7245

A p-value greater than the significance level 0.05 suggests that normality may be assumed.

6. Discussion

Effects of variable frequency on E. Coli TG1

The application of a radiofrequency electric current lacks some characteristics that direct current (DC) treatments have. For example, in the treatment of RFC; none of the existing ions are transported in the surrounding liquid, no new ion is created in the liquid, the electromagnetic fields are not ionizing, it does not produce any electroporation effect, it does not provide free oxygen or other electrolytic substances and, it does not produce a significant heating effect (an increase of 1 ° C on graphene layers, treatment cell, has been reported). At a radio frequency of 10 MHz and with a low intensity like the one we use in the experimental procedure, all these characteristics are met. Meanwhile, treatments such as direct current (DC) modify the pH of the samples, produce and transport additional biocidal ions in the biofilm by an electrophoretic process or produce free oxygen by electrolysis and even produce considerable heating in the samples, being able of causing damage and alteration of the samples (Caubet et al., 2004).

Because the EPS matrix by which the bacterial biofilm is composed has charged polymers (ions) with polar subsystems, whose function is the sorption of other charged molecules involved in cellular interaction, they are considered a target susceptible to the action of treatment RFC base and the influence of electromagnetic fields (Marvasi et al., 2010).

The radiofrequency transmitted through the graphene, conductive layers will vibrate the polar molecules, charged particles, and polar parts of large molecular chains of the biofilm. The vibration will cause the structure of the bacteria to weaken and affect their polarity (Caubet et al., 2004).

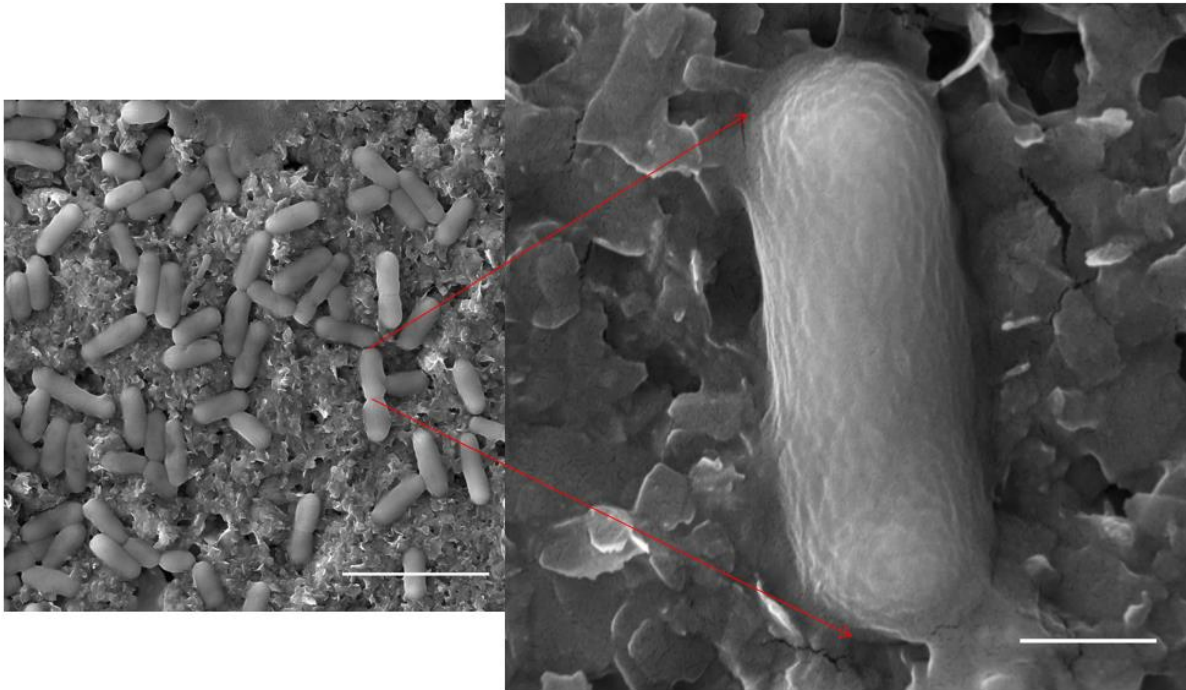
The scanner electron microscopy (SEM) of the variable frequency treatment on the bacteria revealed the cell wall disruption and, subsequently, the cell death. The electromagnetic field affects the oxidoreductive activity of the *E. coli* as well as other biological functions such as changes in enzyme activity, transport of ions, the concentration of hormones, and changes in the synthesis and transcription of DNA (Strašák et al., 2002).

Figure 6. SEM characterization of E. Coli TG1 bacteria

Hv zDFH

Figure 6 shows a magnification of figure 6(c), where the interruption of the cell wall can be observed in two points of the isolated bacteria after 1 hour of treatment based on the radiofrequency application. It should be considered that gram-negative bacteria, such as *E. coli* TG1, have a less hard cell wall than gram-positive ones, and RF-based treatment may not be as effective for this type of bacteria (Nasrabadi et al., 2018).

Figure 7. Magnification of dead E. Coli TG1 bacteria



The literature records cases in the treatment with RFC between 70 kHz and 10 MHz together with the administration of antibiotics. It produces a mechanical effect on the EPS matrix, makes the biofilm vibrate and generates a synergy effect, very similar to the impact Bioelectric. The physical effect produced by the RFC on the biofilm would allow better penetration of the antibiotic (Caubet et al., 2004). In this work, we use variable frequencies of 5 MHz, 10 MHz, and 15 MHz, to evaluate only the physical effect produced on the biofilm and analyze a frequency threshold between the applied frequencies. Future studies will examine the relevance of this work in conjunction with the administration of antibiotics.

7. Conclusions, recommendations, and future work.

7.1 Conclusions

In this investigation, we present the possible application of a radiofrequency treatment as an innovative method of prosthetic sterilization and biofilm formation control. Also, we offer a secure way of preparing thin layers based on graphene, a material that is used to conduct the radiofrequency, and we evaluate their physicochemical properties.

The proposed hypothesis was specifically demonstrated since variable frequencies of 5 MHz, 10 MHz, and 15 MHz will be used on the conductive graphene layers and a percentage of bacterial annihilation of 46.6%, 63.4% and, 73.2%, respectively, will be selected, demonstrating treatment efficacy. The evaluation of the antibacterial effectiveness of this method was performed by; The dilution method and plate count, measuring the optical density at 600 nm, and calculating the colony-forming units (CFU). The statistical analysis proved that there is a threshold between 5MHz and 10MHz in which the treatment begins to be effective. It is beneficial because, at this frequency, there are no factors that alter or damage the samples.

The growth of the bacterial culture was measured from the measurement of optical density (OD). The measurements were made at two different times, at the beginning of the treatment, and 12 hours later. The absorption values after 12 hours exhibit a relevant difference between the control sample and the sample exposed to RFC treatment, compared to the initial samples. This effect was attributed to the application of RFC to create vibration in the graphene layers and the biofilm, making the polar parts charged with the polymeric substances of the biofilm susceptible to the creation of the electromagnetic field and its structure results damaged. These results are promising to develop the application of RFC as an alternative method for the treatment of prosthetic disinfection and prevention of prosthetic biofilm.

7.2 Recommendations and future work

- It is necessary to control the thickness of the graphene thin films and avoid irregularities in the morphology that could cause differences in the conduction of radiofrequency on the layers. To avoid irregularities on the layers surface, the evaporation time of the solvent and the temperature must be calculated, the correct percentage of the graphene solution must be placed, and the ultrasonication times must be maintained to obtain a homogeneous mixture.
- To give uniformity to the layers, this work added PLGA, a copolymer, to give firmness to the layers and to be able to use them in experimentation processes.
- The present study works with *E. coli* TG1, a gram-negative bacterium, usually found in joint prosthetic infection processes, and excellent results were obtained when applying the radiofrequency treatment. However, it is necessary to implement a treatment aimed at other frequent pathogens that cause joint prosthetic infection and perform control tests, and bacterial annihilation analysis, considering the microbiological map and the associated factors that were identified by the present study.
- For future work, it is intended to use external radiofrequency apparatus and radiofrequency ablation on an outpatient basis, by inserting a refrigerated active straight tip electrode, which emits direct electrical energy to the graphene-based prosthesis and allows the creation of an electromagnetic field that affects the polar part of the prosthetic biofilm. This technique is already used in hospitals to treat cancer, osteoid osteoma, breast, thyroid kidney and fibroids, as alternatives to surgery. However, it has not been used for treatments

in prosthetic infections. This treatment is less invasive, with rapid recovery and the patient may return home the same day.

References

- Aliofkhazraei, M., Ali, N., Milne, W. I., Ozkan, C. S., Mitura, S., & Gervasoni, J. L. (2016). *Graphene Science Handbook: Electrical and Optical Properties*. CRC Press.
- Arroyo Rodriguez, C. (2018). *Accessible and cost-effective Method of PDMS Microdevices Fabrication using a reusable Photopolymer Mold*.
<https://onlinelibrary.wiley.com/doi/abs/10.1002/polb.24726?af=R>
- Ayoade, F., & Todd, J. R. (2019). Prosthetic Joint Infection. In *StatPearls*. StatPearls Publishing.
<http://www.ncbi.nlm.nih.gov/books/NBK448131/>
- Bansiddhi, A., Sargeant, T. D., Stupp, S. I., & Dunand, D. C. (2008). Porous NiTi for bone implants: A review. *Acta Biomaterialia*, 4(4), 773–782.
<https://doi.org/10.1016/j.actbio.2008.02.009>
- Cacaci, M., Martini, C., Cinzia, G., Torelli, R., Bugli, F., & Sanguinetti, M. (2019). Graphene Oxide Coatings as Tools to Prevent Microbial Biofilm Formation on Medical Device. *Advances in Experimental Medicine and Biology*.
https://doi.org/10.1007/5584_2019_434
- Caubet, R., Pedarros-Caubet, F., Chu, M., Freye, E., Rodrigues, M. de B., Moreau, J. M., & Ellison, W. J. (2004). *A Radio Frequency Electric Current Enhances Antibiotic Efficacy against Bacterial Biofilms*. 3.
- Cobo, D. (2016). “FACTORES ASOCIADOS AL DESARROLLO DE INFECCIÓN DE PRÓTESIS ARTICULAR EN PACIENTES ATENDIDOS EN EL HOSPITAL DE ESPECIALIDADES N°1 DE LAS FUERZAS ARMADAS, DURANTE EL PERÍODO 2010-2015.
- Esquivias, L., Rivero-Antúnez, P., Zamora-Ledezma, C., Domínguez-Rodríguez, A., & Morales-Flórez, V. (2019). Intragranular carbon nanotubes in alumina-based composites for reinforced ceramics. *Journal of Sol-Gel Science and Technology*, 90(1), 162–171.
<https://doi.org/10.1007/s10971-018-4834-4>
- Flemming, H.-C., & Wingender, J. (2010). The biofilm matrix. *Nature Reviews. Microbiology*, 8(9), 623–633. <https://doi.org/10.1038/nrmicro2415>
- Franco-Cendejas, R., Contreras-Córdova, E. L., Mondragón-Eguiluz, J. A., Vanegas-Rodríguez, E. S., Ilizaliturri-Sánchez, V. M., & Galindo-Fraga, A. (2017). Incidencia de infecciones protésicas primarias de cadera y rodilla en un centro de la Ciudad de México. *Cirugía y Cirujanos*, 85(6), 485–492. <https://doi.org/10.1016/j.circir.2016.10.032>
- Ghughe, A. D., Shirode, A. R., & Kadam, V. J. (2017). Graphene: A Comprehensive Review. *Current Drug Targets*, 18(6), 724–733.
<https://doi.org/10.2174/1389450117666160709023425>
- Gilbertie, J. M., Schnabel, L. V., Hickok, N. J., Jacob, M. E., Conlon, B. P., Shapiro, I. M., Parvizi, J., & Schaer, T. P. (2019). Equine or porcine synovial fluid as a novel ex vivo model for the study of bacterial free-floating biofilms that form in human joint infections. *PLOS ONE*, 14(8), e0221012. <https://doi.org/10.1371/journal.pone.0221012>

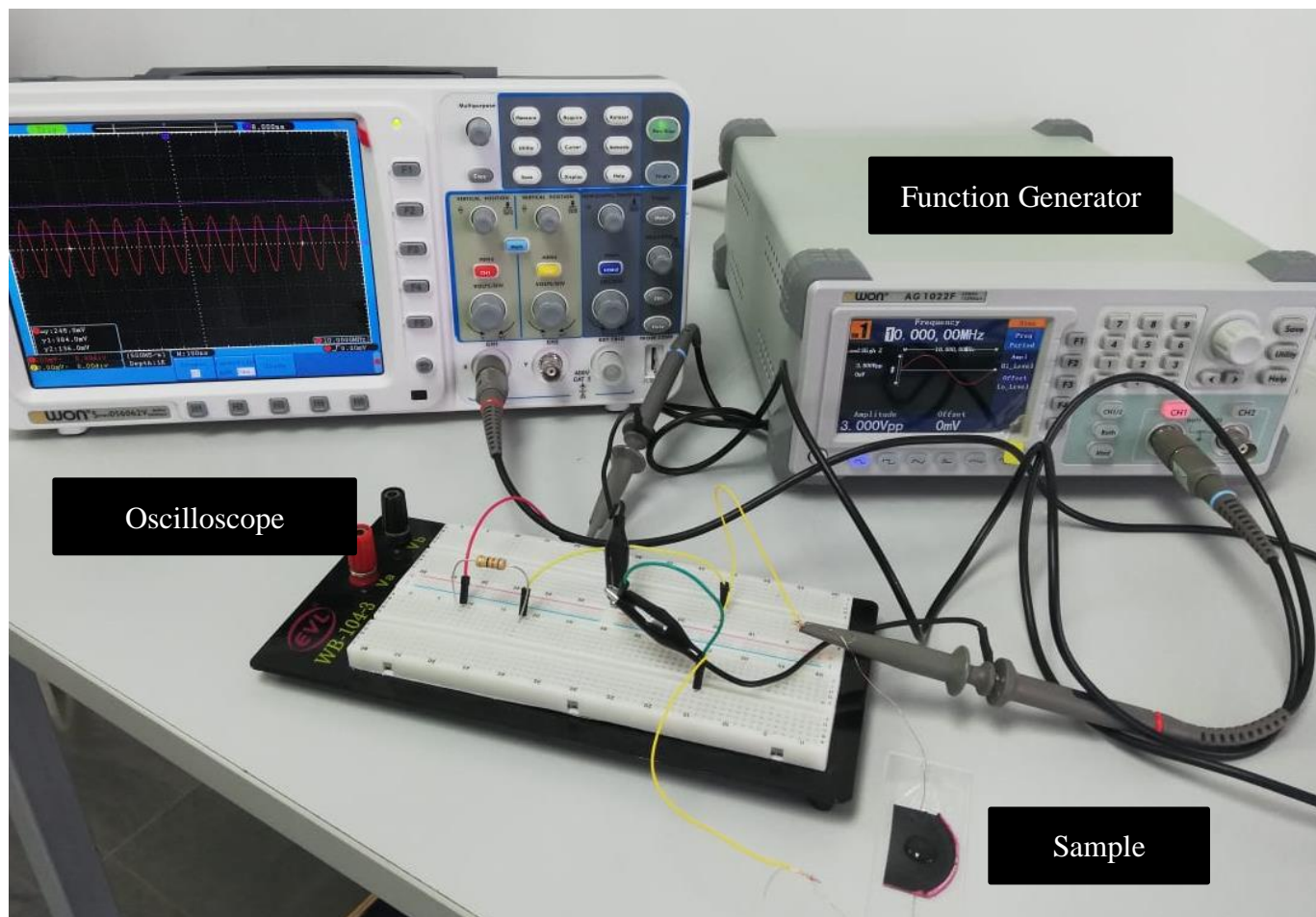
- Heller, E. J., Yang, Y., Kocia, L., Chen, W., Fang, S., Borunda, M., & Kaxiras, E. (2016). Theory of Graphene Raman Scattering. *ACS Nano*, *10*(2), 2803–2818. <https://doi.org/10.1021/acsnano.5b07676>
- Herigstad, B., Hamilton, M., & Heersink, J. (2001). How to optimize the drop plate method for enumerating bacteria. *Journal of Microbiological Methods*, *44*(2), 121–129. [https://doi.org/10.1016/S0167-7012\(00\)00241-4](https://doi.org/10.1016/S0167-7012(00)00241-4)
- Kiedrowski, M. R., & Horswill, A. R. (2011). New approaches for treating staphylococcal biofilm infections. *Annals of the New York Academy of Sciences*, *1241*, 104–121. <https://doi.org/10.1111/j.1749-6632.2011.06281.x>
- Kim, H., Abdala, A. A., & Macosko, C. W. (2010). Graphene/Polymer Nanocomposites. *Macromolecules*, *43*(16), 6515–6530. <https://doi.org/10.1021/ma100572e>
- Kostarelos, K., & Novoselov, K. S. (2014). Exploring the Interface of Graphene and Biology. *Science*, *344*(6181), 261–263. <https://doi.org/10.1126/science.1246736>
- Lamagni, T. (2014). Epidemiology and burden of prosthetic joint infections. *Journal of Antimicrobial Chemotherapy*, *69*(suppl_1), i5–i10. <https://doi.org/10.1093/jac/dku247>
- Lazzeri, M. (2012). *Application of raman spectroscopy to the study of graphitic carbons in the earth sciences*. https://www.researchgate.net/publication/286098532_Application_of_raman_spectroscopy_to_the_study_of_graphitic_carbons_in_the_earth_sciences
- Liu, Y., Shi, L., Su, L., Mei, H. C. van der, Jutte, P. C., Ren, Y., & Busscher, H. J. (2019). Nanotechnology-based antimicrobials and delivery systems for biofilm-infection control. *Chemical Society Reviews*, *48*(2), 428–446. <https://doi.org/10.1039/C7CS00807D>
- Lodish, H., Berk, A., Zipursky, S. L., Matsudaira, P., Baltimore, D., & Darnell, J. (2000). Growth of Microorganisms in Culture. *Molecular Cell Biology*. 4th Edition. <https://www.ncbi.nlm.nih.gov/books/NBK21593/>
- López-Santos, C., Terriza, A., Portolés, J., Yubero, F., & González, A. R. (2015). *Physiological Degradation Mechanisms of PLGA Membrane Films under Oxygen Plasma Treatment / The Journal of Physical Chemistry C*. <https://pubs.acs.org/doi/abs/10.1021/acs.jpcc.5b05011>
- Marvasi, M., Visscher, P. T., & Casillas Martinez, L. (2010). Exopolymeric substances (EPS) from *Bacillus subtilis*: Polymers and genes encoding their synthesis. *FEMS Microbiology Letters*, *313*(1), 1–9. <https://doi.org/10.1111/j.1574-6968.2010.02085.x>
- McConoughey, S., Howlin, R., Granger, J., Manring, M., Calhoun, J., Shirtliff, M., Kathju, S., & Stoodley, P. (2014). *Biofilms in periprosthetic orthopedic infections*. *9*(8), 987–1007. <https://doi.org/10.2217/FMB.14.64>
- Meric, I., Han, M. Y., Young, A. F., Ozyilmaz, B., Kim, P., & Shepard, K. L. (2008). Current saturation in zero-bandgap, top-gated graphene field-effect transistors. *Nature Nanotechnology*, *3*(11), 654–659. <https://doi.org/10.1038/nnano.2008.268>
- Murata, H., Nakajima, Y., Saitoh, N., Yoshizawa, N., Suemasu, T., & Toko, K. (2019). High-Electrical-Conductivity Multilayer Graphene Formed by Layer Exchange with Controlled Thickness and Interlayer. *Scientific Reports*, *9*(1), 1–5. <https://doi.org/10.1038/s41598-019-40547-0>

- Nasrabadi, A. M., An, S., Kwon, S.-B., & Hwang, J. (2018). Investigation of live and dead status of airborne bacteria using UVAPS with LIVE/DEAD® BacLight Kit. *Journal of Aerosol Science*, *115*, 181–189. <https://doi.org/10.1016/j.jaerosci.2017.10.012>
- Nielsen, R. K., Egund, N., Jørgensen, A., & Jurik, A. (2017). *Risk factors for joint replacement in knee osteoarthritis; a 15-year follow-up study*. *18*((1)). <https://doi.org/10.1186/s12891-017-1871-z>
- Oliete, J. B., Oltra, T. M., Sánchez, M. Á. A., García, F. B., Sabaté, E. F., & Lanzuela, M. F. (2015). *Aproximación Actual a la Infección Protésica*.
- Pandit, S., Cao, Z., Mokkalapati, V. R. S. S., Celauro, E., Yurgens, A., Lovmar, M., Westerlund, F., Sun, J., & Mijakovic, I. (2018). Vertically Aligned Graphene Coating is Bactericidal and Prevents the Formation of Bacterial Biofilms. *Advanced Materials Interfaces*, *5*(7), 1701331. <https://doi.org/10.1002/admi.201701331>
- Papageorgiou, D. G., Kinloch, I. A., & Young, R. J. (2017). Mechanical properties of graphene and graphene-based nanocomposites. *Progress in Materials Science*, *90*, 75–127. <https://doi.org/10.1016/j.pmatsci.2017.07.004>
- Peleias Junior, F. dos S., Zeituni, C. A., Rostelato, M. E. C. M., Fechine, G. J. M., Souza, C. D. de, Mattos, F. R. de, Santana de Moura, E., Moura, J. A., Benega, M. A. G., Feher, A., Costa, O. L. da, & Rodrigues, B. T. (2015). Desenvolvimento da metodologia para síntese do poli(ácido láctico-co-ácido glicólico) para utilização na produção de fontes radioativas. *Polímeros*, *25*(3), 317–325. <https://doi.org/10.1590/0104-1428.1428>
- Podila, R., Moore, T., Alexis, F., & Rao, A. (2013). Graphene Coatings for Biomedical Implants. *Journal of Visualized Experiments*, *73*, 50276. <https://doi.org/10.3791/50276>
- R Core Team. (2018). *R: A language and environment for statistical computing*. R Core Team. <https://www.R-project.org/>
- Sebastian, S., Malhotra, R., & Dhawan, B. (2018). Prosthetic joint infection: A major threat to successful total joint arthroplasty. *Indian Journal of Medical Microbiology*, *36*(4), 475. https://doi.org/10.4103/ijmm.IJMM_19_11
- Shahil, K. M. F., & Balandin, A. A. (2012). Thermal properties of graphene and multilayer graphene: Applications in thermal interface materials. *Solid State Communications*, *152*(15), 1331–1340. <https://doi.org/10.1016/j.ssc.2012.04.034>
- Shin, K.-Y., Hong, J.-Y., Lee, S., & Jang, J. (2012). *High electrothermal performance of expanded graphite nanoplatelet-based patch heater—Journal of Materials Chemistry (RSC Publishing)*. <https://pubs.rsc.org/en/content/articlelanding/2012/jm/c2jm34196d#!divAbstract>
- Singh, S. P., Li, Y., Be'er, A., Oren, Y., Tour, J. M., & Arnusch, C. J. (2017). Laser-Induced Graphene Layers and Electrodes Prevents Microbial Fouling and Exerts Antimicrobial Action. *ACS Applied Materials & Interfaces*, *9*(21), 18238–18247. <https://doi.org/10.1021/acsami.7b04863>
- Strašák, L., Vetterl, V., & Šmarda, J. (2002). Effects of low-frequency magnetic fields on bacteria *Escherichia coli*. *Bioelectrochemistry*, *55*(1), 161–164. [https://doi.org/10.1016/S1567-5394\(01\)00152-9](https://doi.org/10.1016/S1567-5394(01)00152-9)
- Taha, M., Abdelbary, H., Ross, F. P., & Carli, A. V. (2018). New Innovations in the Treatment of PJI and Biofilms—Clinical and Preclinical Topics. *Current Reviews in Musculoskeletal Medicine*, *11*(3), 380–388. <https://doi.org/10.1007/s12178-018-9500-5>

- Tande, A. J., & Patel, R. (2014). Prosthetic joint infection. *Clinical Microbiology Reviews*, 27(2), 302–345. <https://doi.org/10.1128/CMR.00111-13>
- Taylor, E. N., & Webster, T. J. (n.d.). For prosthetic biofilm prevention. *International Journal of Nanomedicine*, 8.
- Torres, M., & Enrique, M. (2018). *Prevalencia de complicaciones tempranas en pacientes sometidos artroplastia total de rodilla atendidos en Traumatología, Hospital Eugenio Espejo, Enero 2013 a Diciembre 2016*. <http://www.dspace.uce.edu.ec/handle/25000/16137>
- Torres-Canas, F. J., Blanc, C., Zamora-Ledezma, C., Silva, P., & Anglaret, E. (2015). Dispersion and Individualization of SWNT in Surfactant-Free Suspensions and Composites of Hydrosoluble Polymers. *The Journal of Physical Chemistry C*, 119(1), 703–709. <https://doi.org/10.1021/jp5092015>
- Webster, T. J. (2009). The use of superparamagnetic nanoparticles for prosthetic biofilm prevention. *International Journal of Nanomedicine*, 145. <https://doi.org/10.2147/IJN.S5976>
- Yang, H., Hernandez, Y., Schlierf, A., Felten, A., Eckmann, A., Johal, S., Louette, P., Pireaux, J.-J., Feng, X., Mullen, K., Palermo, V., & Casiraghi, C. (2013). A simple method for graphene production based on exfoliation of graphite in water using 1-pyrenesulfonic acid sodium salt. *Carbon*, 53, 357–365. <https://doi.org/10.1016/j.carbon.2012.11.022>
- Yao, W., & Fan, L. (2019). The Effect of Ion Irradiation Induced Defects on Mechanical Properties of Graphene/Copper Layered Nanocomposites. *Metals*, 9(7), 733. <https://doi.org/10.3390/met9070733>

Annex A

Figure 8. Variable frequency experimental set up used to stimulate bacteria.



Annex B

Figure 9. Method of dilution method and plate colony count.

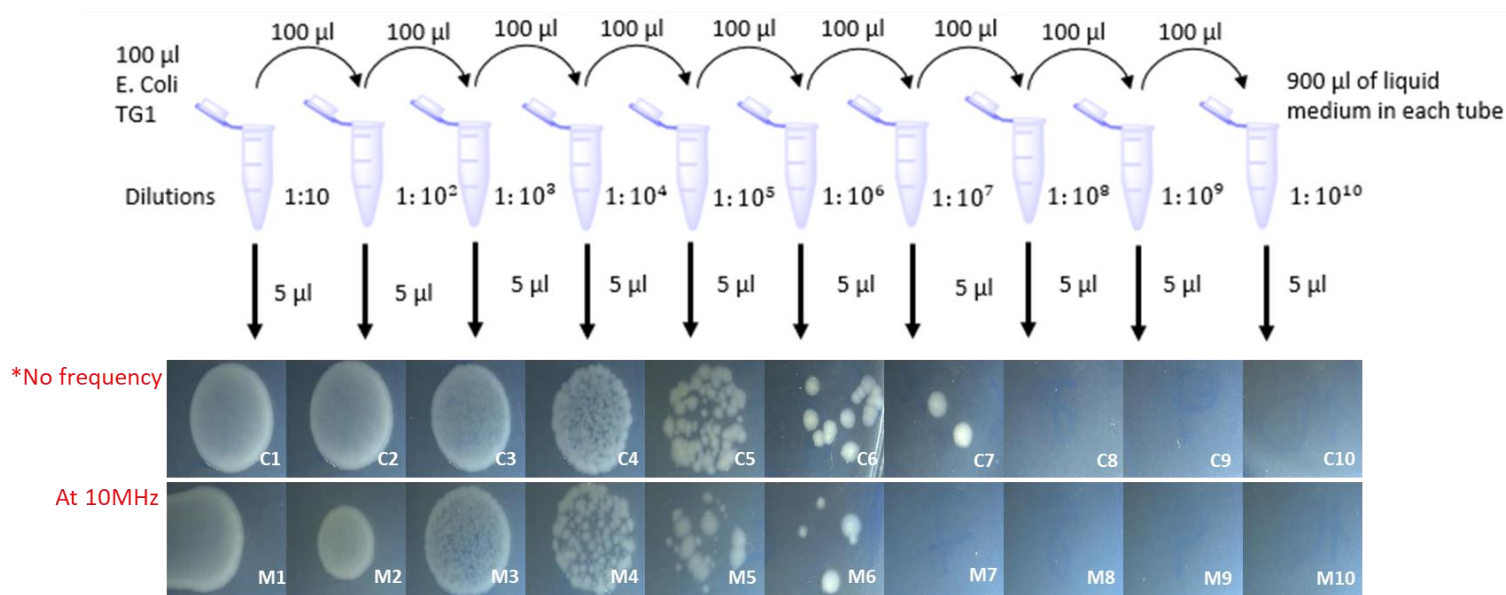
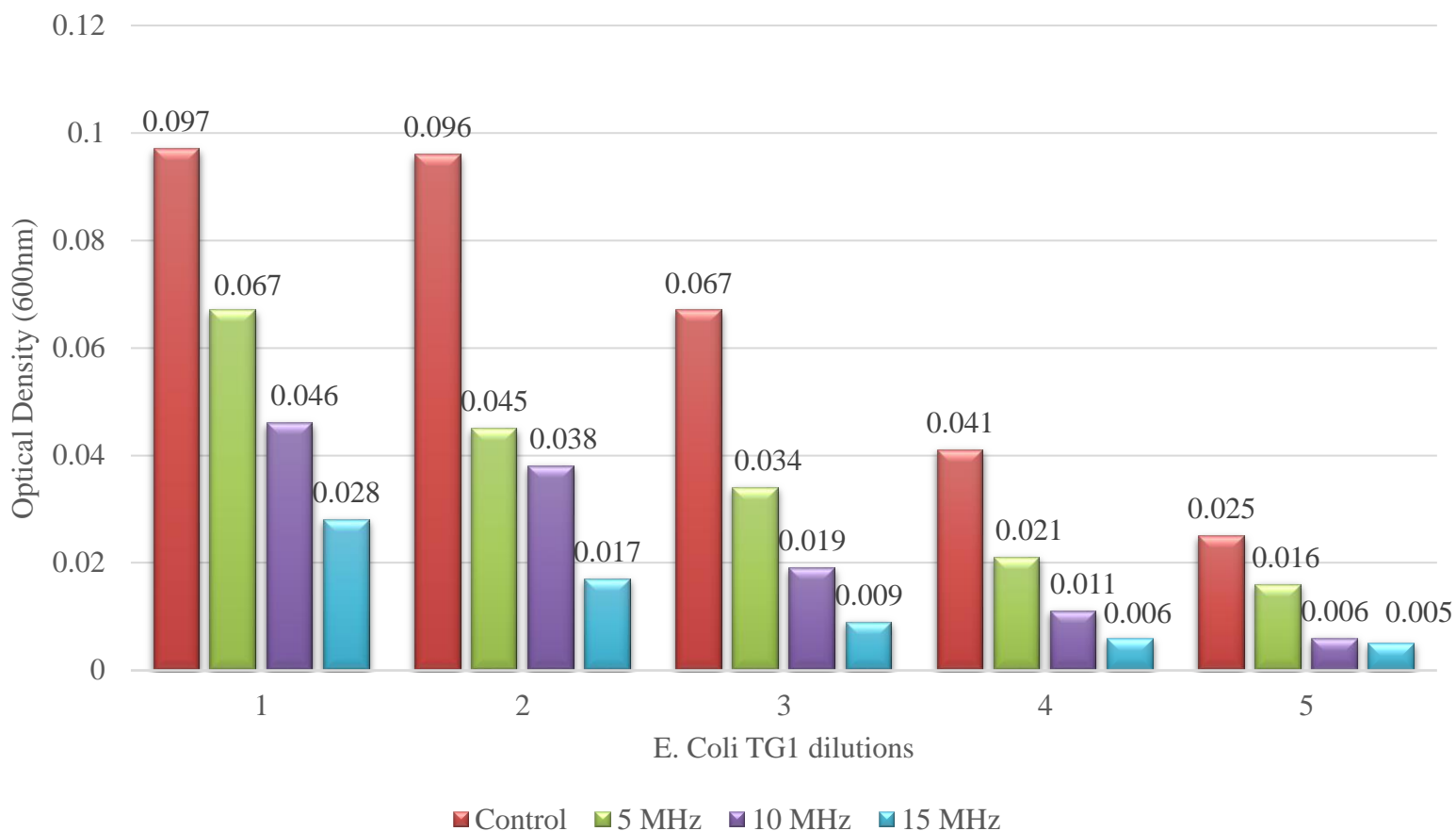


Table 14. Optical Density values for each dilution at different frequency treatments

Dilutions	Control	5MHz	10MHz	15MHz
1	0.097	0.067	0.046	0.028
2	0.096	0.045	0.038	0.017
3	0.067	0.034	0.019	0.009
4	0.041	0.021	0.011	0.006
5	0.025	0.016	0.006	0.005

Graph 10. Representation of the OD values at 600 nm for each dilution at different frequency**treatments****Annex C****CODE:****Statistical Analysis R.**

```

#Reading data (.../Data 12hours.csv)
data<-read.csv(file.choose())
#Installing packages if required
if(!require(dplyr)) install.packages("dplyr")
if(!require(car)) install.packages("car")
#Displaying levels(treatments)
levels(data$Frequency)

```

```

#Ordering levels to ease visualization
data$Frequency <- ordered(data$Frequency,levels = c("0 (Control)", "5", "10", "15"))
#Computing relevant information from different groups of observations:
#mean, standard deviation(sd), and amount of observations per group(count)
library(dplyr)
group_by(data,Frequency)%>%
summarise(count=n(),
           mean=mean(Absorbance,na.rm=TRUE),
           sd=sd(Absorbance, na.rm= TRUE))
#Visualizing data
boxplot(Absorbance~Frequency, data=data,
        xlab="Frequency (MHz)", ylab="Absorbance (nm)",
        frame=FALSE,col=c("#E0FFFF", "#82CAFF", "#157DEC", "#0041B0" ))
#Computing one-way ANOVA test
res.aov <- aov(Absorbance ~ Frequency, data = data)

#Summary of the analysis
summary(res.aov)
#Pairwise-comparison between means of treatment groups
TukeyHSD(res.aov)
#Testing assumptions (validity of ANOVA test)
# 1. Homogeneity of variances
library(car)
leveneTest(Absorbance ~ Frequency, data = data)
# 2. Normality
aov_residuals <- residuals(object = res.aov )
shapiro.test(x = aov_residuals )

```

Table 15. Raw Data used for the statistical analysis in R

Absorbance	Frequency
0.097	0 (Control)
0.096	0 (Control)
0.067	0 (Control)
0.041	0 (Control)
0.025	0 (Control)
0.067	5
0.045	5

0.034	5
0.021	5
0.016	5
0.046	10
0.038	10
0.019	10
0.011	10
0.006	10
0.028	15
0.017	15
0.009	15
0.006	15
0.005	15